MINIMAL BOUNDARY CONDITIONS FOR SIMULATIONS OF DISORDERED MATERIALS

By

JAGAN PADBIDRI

A thesis submitted in partial fulfillment of
the requirements for the degree of

MASTER OF SCIENCE IN MECHANICAL ENGINEERING

WASHINGTON STATE UNIVERSITY
School of Mechanical and Materials Engineering

December 2003

To the Faculty of Washington State University:

The members of the Committee appointed to examine the thesis of JAGAN PADBIDRI find it satisfactory and recommend that it be accepted.

_____

Chair

_____

_____

ACKNOWLEDGEMENT

I would like to thank my committee chair and advisor Dr. Sinisa Mesarovic under whose guidance this research was conducted. He has continuously supported me in times of need providing fresh ideas and useful insights. I would also like to thank my other committee members Dr. Hussein Zbib and Dr. David Field for being in my committee and providing helpful suggestions.

I would also like to thank my friends Ravindra Akarapu, Rajesh Prasannavenkatesan and my office mates Firas Akasheh, Mutasem Shehadeh and Shafique Khan at ETRL 130 for all the helpful and interesting discussions we have had regarding this research. I would also like to acknowledge the financial support received from the School of Mechanical and Materials Engineering, WSU for the completion of my degree.

MINIMAL BOUNDARY CONDITIONS FOR SIMULATIONS OF

DISORDERED MATERIALS

Abstract

By Jagan Padbidri, M.S.
Washington State University
December 2003

Chair: Sinisa Dj. Mesarovic

Traditional boundary conditions impose artificial rigidity and/or periodicity on the Representative Volume Element (RVE) during deformation simulations of materials. The result is a very small portion of the computational model demonstrates the actual microstructural state of the deformation. These are referred to as End Effects and lead to computational inefficiency. Further, they introduce Spurious wavelengths in the field variables.

The current research presents the development of Minimal boundary conditions and their implementation to an elastic crystalline aggregate. The Minimal boundary conditions do not impose any rigidity or periodicity on the computational model and effectively eliminate the problem of End Effects. The simulations are carried out on polycrystalline aggregates of different sizes and for different realizations of the orientations of the grains constituting the aggregate.

The superiority of the Minimal boundary conditions is demonstrated by subjecting the same aggregate to the other traditional boundary conditions and gauging the overall

elastic response. The Minimal boundary conditions deform the material such that the overall response falls within the Hashin-Shtrikman bounds for the elastic constants of an infinite polycrystal assembly.

A two-dimensional Fourier Transform of the field variables illustrates that the Minimal boundary conditions contribute Spurious wavelengths to a far lesser extent than the traditional boundary conditions.

TABLE OF CONTENTS

LIST OF FIGURES

LIST OF TABLES

CHAPTER 1

INTRODUCTION

1.1 Disordered Materials

Modeling and simulation of disordered materials is having an increasing impact on understanding of the behavior of materials, both, in the processing stage and in service. Examples of disordered structures of materials can be found on all length scales viz. granular materials (Fig. 1.1 a), metallic foams (Fig.1.1 b) etc. on the macro-scale, polycrystalline materials (Fig.1.1 c), fine powders as in powder metallurgy etc. on the micro-scale.

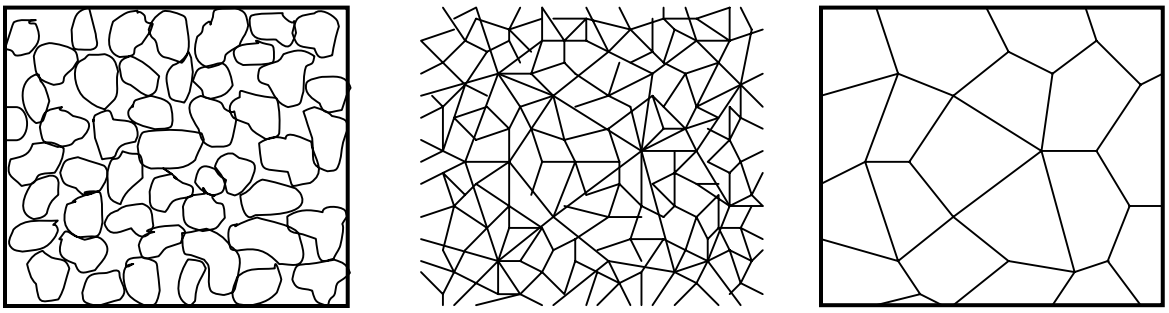

(a) (b) (c)

Fig. 1.1 Disordered Materials

The challenge is to relate the macroscopically imposed strain/stress with the resultant microscopic variables. These microscopic variables could be the contact forces for a granular material, the tensile or compressive stresses developed in the minute beams of the metallic foam or the stresses or strains developed at a microscopic scale in a polycrystalline aggregate. The problem is complicated due to the heterogeneity of the material.

Further, the accuracy of the analysis technique assumes great importance since the variables imposed are at the macroscopic length scale, but the variables analyzed are at

the microscopic length scale. The computational modeling of the material should overcome the properties inherent to a macroscopic modeling such as free surfaces. Modeling and simulations of disordered materials are usually done for a representative volume element (RVE). The RVE is an assembly of basic building blocks i.e. atoms, grains, granules, etc. It is assumed that such element of volume is representative of the materials' behavior at large. For the purpose of simulation, it serves as a quasi-unit cell. The RVE is then subjected to boundary conditions (BC's), and the behavior of the disordered assembly observed.

1.2 The Representative Volume Element

One important goal of the mechanics and physics of heterogeneous materials is to derive their effective properties from the knowledge of the constitutive laws and spatial distributions of their components. Homogenization methods have been designed for this purpose which have reached a high level of sophistication and accuracy particularly for linear properties such as elasticity.

Rigorous bounds for the macroscopic linear properties of composites are available. These include the Voigt-Reuss bounds and the Hashin-Shtrikman bounds. These estimations are given for a random composite media with an infinite extension and, hence, are asymptotic estimates. A different method to solve homogenization problems is to use numerical techniques and simulations on samples of microstructure. This renders the notion of Representative Volume Element (RVE) very important.

The RVE is usually regarded as a volume of heterogeneous material that is sufficiently large to be statistically representative of the composite i.e. it effectively

includes a sampling of all the microscopic heterogeneities that can occur in the composite. Another definition provided by Drugan and Willis (1996) states that an RVE is the smallest material element volume of a composite for which the usual spatially constant (overall modulus) macroscopic constitutive representation is a sufficiently accurate model to represent the mean constitutive response. This approach uses the principle of homogenization for an infinite medium and does not take into account the statistical fluctuations of effective properties over finite domains.

These definitions lead to the fact that the RVE must include a large number of micro-heterogeneities of the composite. Several types of boundary conditions can be prescribed on the RVE to impose a given mean strain or mean stress to the given material element.

The response of an RVE has to be independent of the nature of the boundary conditions. This would require an enormous size of the RVE. This is due to the excessive constraints imposed on the RVE for the simulations. This problem is overcome by the Minimal Boundary conditions, thus rendering a more manageable size of the RVE. The boundary conditions used traditionally and their drawbacks are outlined in the succeeding section.

1.3 Traditional Boundary Conditions

The most commonly used boundary conditions are Rigid boundary conditions (Fig 1.2 (a)) and Periodic boundary conditions (Fig. 1.2 (b)). The Rigid boundary conditions impose a rigid boundary and periodicity. The Periodic boundary condition is

slightly more relaxed, in that, only periodicity is applied. The boundary conditions are shown below.

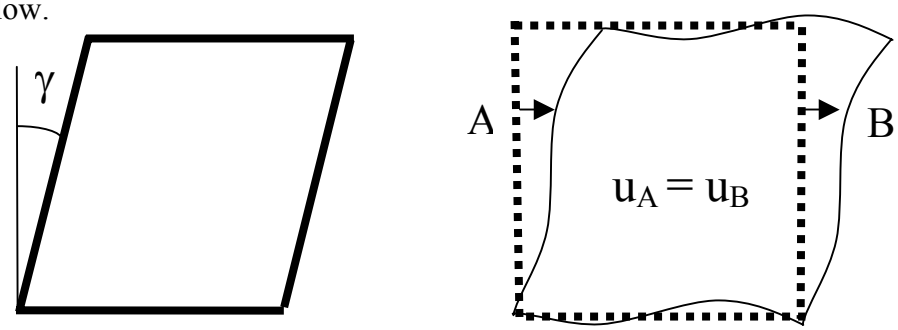

Fig. 1.2 Rigid and Periodic boundary conditions

The Periodic boundary condition is more commonly used. The rigid boundary condition is simpler to use, but is rarely used. In the strict sense, both periodic and rigid boundary conditions are wrong. There is no reason to assume that a disordered RVE will act as a periodic unit cell. The additional restrictions in the boundary conditions cause boundary effects, so that the "useful volume" of the smaller then the volume of the simulated volume. The additional constraint results in a stiff response. Moreover, the enforced periodicity adds artificial wavelengths to the solution fields, of the order of the cell size. Some important features of materials' behavior will not be predicted by such simulations.

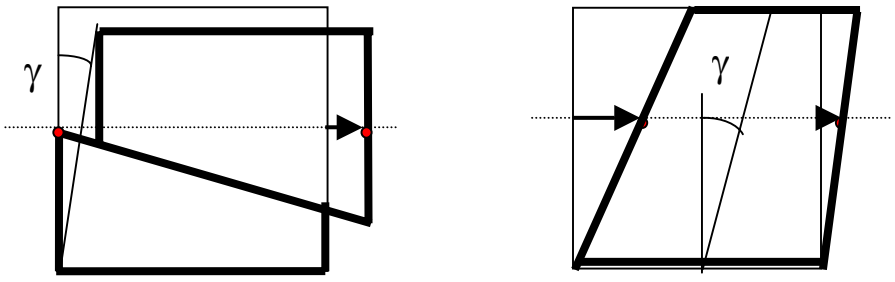

Fig. 1.3 Rigid and Periodic BCs prevent Strain Localization and Strain Gradients

Both periodic and rigid boundary conditions will prevent localization and development of strain gradients depicted in the figure above.

1.4 Objective and Approach of the current research

The objective of the current research is to implement new Minimal boundary conditions which overcome the aforementioned defects. These boundary conditions use a definition of strain provided by Bishop and Hill (1951) defining the macroscopic strain as the volumetric average of strain in the body. This is reduced to a lower order integral and implemented using Finite Elements.

The test case considered is a Linear Elastic problem for a two-dimensional aggregate of crystals. The average strain defined over the area is reduced to an integral over the boundary and then as a summation of products of the normals to the boundary and displacements of the nodes on the boundary. In a Linear Elastic case, the direction of the normal of the boundary is considered to remain the same during the entire process of deformation. This renders the Linear Elastic case easy for implementation. The concept is extendable to Non-Linear cases as well where the boundary conditions are applied incrementally.

A polycrystalline aggregate is simulated and the different boundary conditions are applied to it. The overall response and the presence of spurious wavelengths are verified using Fourier Transforms. The minimal boundary conditions are expected to yield leaner results than the rigid or periodic boundary conditions since nothing but the strain is imposed in this case. Bounds are derived for the overall elastic response of a polycrystal. The derivation of the bounds is presented in detail in the next chapter.

CHAPTER 2

HASHIN-SHTRIKMAN BOUNDS FOR THE ELASTIC MODULUS OF A CRYSTALLINE AGGREGATE

Variational principles for anisotropic elasticity were applied to the derivation of bounds for the elastic modulii of polycrystals in terms of the modulus of the constituting crystals by Hashin Z and Shtrikman S (1962).

Consider a homogenous, isotropic elastic body of volume V and surface S. Let this body be deformed so that the surface displacements are given by

$$u_i^S(S) = \varepsilon_{ij}^0 x_j \tag{2.2.1}$$

Since the body is homogenous and isotropic, the strain field throughout the body is homogenous and given by ε_{ij}^0. Also, the displacement field inside the body is known. Let this be represented by u_{ij}^0 which is related to ε_{ij}^0 by the usual small strain expression.

Consider a polycrystalline body with randomly oriented crystals. A cubical element is selected from this body which is large when compared to the individual crystals but small when compared to the body as a whole. The mean strains in this cubical element will be the same as those for the entire body. This cubical element will be henceforth referred to as a reference cube. Let the same surface displacements as in (2.2.1) be prescribed on the polycrystalline body. The strains in the reference cube will be given by

$$\varepsilon_{ij} = \varepsilon_{ij}^0 + \varepsilon'_{ij} \tag{2.2.2}$$

where ε'_{ij} are deviations from the mean strain and its average over the entire volume is 0. The displacement field in this body, u_i, will be different from that of the homogenous body due to the anisotropy.

The stress field in the homogenous body is given by

$$\sigma^0_{ij} = C^0_{ijkl}\varepsilon^0_{kl} \tag{2.2.3}$$

where for the present homogenous case

$$C^0_{ijkl} = \lambda_0\delta_{ij}\delta_{kl} + 2G_0 I_{ijkl} \tag{2.2.4}$$

where λ_0 and G_0 are the Lame and Shear modulus respectively, which are constant in space. The tensor *I* is defined as

$$I_{ijkl} = \frac{1}{2}\left(\delta_{ik}\delta_{jl} + \delta_{il}\delta_{jk}\right) \tag{2.2.5}$$

The stress-strain relation for the anisotropic material is given by

$$\sigma_{ij} = C_{ijkl}\varepsilon_{kl} \tag{2.2.6}$$

where the components of C_{ijkl} are variable in space, but satisfy the usual symmetry relations.

Define

$$u'_i = u_i - u^0_i \tag{2.2.7}$$

$$\varepsilon'_{ij} = \varepsilon_{ij} - \varepsilon^0_{ij} \tag{2.2.8}$$

and the symmetric stress polarization tensor as

$$p_{ij} = \sigma_{ij} - C^0_{ijkl}\varepsilon_{kl} \tag{2.2.9}$$

Let the tensor *R* be defined as

$$R_{ijkl} = C_{ijkl} - C^0_{ijkl} \tag{2.2.10}$$

and the tensor H as the reciprocal of R so that

$$H_{ijmn} R_{mnkl} = I_{ijkl} \tag{2.2.11}$$

The ε'_{ij} and p_{ij} are chosen as unknowns here and variational principles in terms of these quantities are formulated.

Consider the integral

$$U_p = \frac{1}{2}\int_V \sigma^0_{ij}\varepsilon^0_{ij} dV - \frac{1}{2}\int_V \left(H_{ijkl} p_{ij} p_{kl} - p_{ij}\varepsilon'_{ij} - 2p_{ij}\varepsilon^0_{ij}\right) dV \tag{2.2.12}$$

subject to the condition

$$\left(C^0_{ijkl}\varepsilon'_{kl} + p_{ij}\right)_{,j} = 0 \tag{2.2.13}$$

and the boundary condition

$$u'_i \left(S\right) = 0 \tag{2.2.14}$$

The first variation of Up is given by

$$\delta U_p = -\frac{1}{2}\int_V \left[2\left(H_{ijkl} p_{kl} - \varepsilon_{ij}\right)\delta p_{ij} + \varepsilon'_{ij}\,\delta p_{ij} - p_{ij}\delta\varepsilon'_{ij}\right] dV \tag{2.2.15}$$

Let the condition given in (2.2.13) be integrated in the form

$$C^0_{ijkl}\varepsilon'_{kl} + p_{ij} = t_{ij} \tag{2.2.16}$$

where $t_{ij,j} = 0$. (2.2.17)

The variations of (2.2.16) and (2.2.17) are

$$C^0_{ijkl}\delta\varepsilon'_{kl} + \delta p_{ij} = \delta t_{ij} \tag{2.2.18}$$

and $\delta t_{ij,j} = 0$. (2.2.19)

consider the part of (2.2.15) given by

$$\int_V (\varepsilon'_{ij}\ \delta p_{ij}\ -\ p_{ij}\delta\varepsilon'_{ij}\ )dV$$

Substituting the values of p_{ij} and $\delta p_{ij,j}$ from (2.2.16) and (2.2.17), we get

$$\int_V \left[\varepsilon'_{ij}\ \left(\delta t_{ij}\ -\ C^0_{ijkl}\delta\varepsilon'_{kl}\right) - \left(t_{ij}\ -\ C^0_{ijkl}\varepsilon'_{kl}\right)\delta\varepsilon'_{ij}\right]dV$$

$$= \int_V \left(\varepsilon'_{ij}\ \delta t_{ij}\ - t_{ij}\delta\varepsilon'_{ij} - \varepsilon'_{ij}\ C^0_{ijkl}\delta\varepsilon'_{kl} + \delta\varepsilon'_{ij}\ C^0_{ijkl}\varepsilon'_{kl}\right)dV$$

the last two terms cancel due to the symmetry of C^0_{ijkl}. This reduces the integral to

$$\int_V \left(\varepsilon'_{ij}\ \delta t_{ij}\ - t_{ij}\delta\varepsilon'_{ij}\right)dV$$

$$= \frac{1}{2}\int_V \left(u'_{i,j}\ \delta t_{ij}\ + u'_{j,i}\ \delta t_{ij}\ - t_{ij}\delta u'_{i,j} - t_{ij}\delta u'_{j,i}\right)dV$$

$$= \frac{1}{2}\left[\int_S \delta t_{ij}u'_i\ n_j dS - \int_V \delta t_{ij,j}u'_i\ dV\right] + \frac{1}{2}\left[\int_S \delta t_{ij}u'_j\ n_i dS - \int_V \delta t_{ij,i}u'_j\ dV\right]$$
$$- \frac{1}{2}\left[\int_S t_{ij}\delta u'_i\ n_j - \int_V t_{ij,j}\delta u'_i\right] - \frac{1}{2}\left[\int_S t_{ij}\delta u'_j\ n_i - \int_V t_{ij,i}\delta u'_j\right]$$

the above integral reduces to 0 since $u'_i\ (S) = 0$, $\delta t_{ij,j} = 0$ and $t_{ij,j} = 0$ on V.

So, of the original integral equation given by (2.2.15), the part that remains is

$$\delta U_p = -\frac{1}{2}\int_V \left[2\left(H_{ijkl}p_{kl} - \varepsilon_{ij}\right)\delta p_{ij}\right]dV$$

This also reduces to 0 when

$$H_{ijkl}p_{kl} - \varepsilon_{ij} = 0$$

$$\Rightarrow \; p_{ij} \; = \; R_{ijkl}\varepsilon_{kl} \qquad (2.2.20)$$

i.e. $\delta U_p \; = \; 0$ for the above condition. This means that U_p attains a stationary, extremal value denoted by U_p^s. It can be demonstrated that U_p^s is the actual strain energy stored in the body. Its value is an absolute maximum when R_{ijkl} is positive definite and an absolute minimum when R_{ijkl} is negative definite.

When the C_{ijkl}^0 are very small when compared to the C_{ijkl}, the variational principles reduce to the principle of minimum complimentary energy, whereas when the C_{ijkl}^0 are infinitely large when compared to C_{ijkl}, the principle of minimum potential energy is obtained.

The strain energy stored in a reference cube, when (2.2.1) is prescribed on the boundary of the body is given by

$$U \; = \; \frac{1}{2}\left(9K^*\left(\varepsilon^0\right)^2 \; + \; 2G^* e_{ij}^0 e_{ij}^0\right) \qquad (2.2.21)$$

where K^* and G^* are the effective bulk and shear modulii respectively, $\varepsilon^0 \; = \; \frac{1}{3}\,\varepsilon_{kk}^0$ and

$e_{ij}^0 \; = \; \varepsilon_{ij}^0 \; - \; \varepsilon^0 \delta_{ij}$

Let the orientation of the Cartesian crystallographic axes of a crystal with respect to the fixed Cartesian co-ordinate system be denoted by Ω. The volume of all crystals with the same orientation is given by V_Ω. Since the number of crystals is very large and Ω is taken as continuous,

$$V_\Omega \; = \; Vd\Omega \; = \; dV \qquad (2.2.22)$$

Since the polarization field can be arbitrarily chosen, due to the variational formulation, a piecewise constant field is chosen in V_Ω. Since the orientations are continuous, this can be written as

$p_{ij} = p_{ij}(\Omega)$ where p_{ij} are continuous functions of Ω. The orientation average of the polarization function is given by

$$< p_{ij} >= \int p_{ij}(\Omega) d\Omega \text{ where } \int d\Omega = 1 \qquad (2.2.23)$$

The integral in (2.2.12) for the reference cube can now be written in terms of $p_{ij}(\Omega)$ as

$$U_p = U_0 + U' - \frac{1}{2}\int \left[H_{ijkl}(\Omega) p_{ij}(\Omega) p_{kl}(\Omega) - 2 p_{ij}(\Omega)\varepsilon^0_{ij}\right] d\Omega \qquad (2.2.24)$$

where $U' = \frac{1}{2}\int p_{ij}(\Omega)\varepsilon'_{ij}(\Omega) d\Omega$

expressing p_{ij} and u'_i as Fourier series and substituting them in (2.2.13), we get

$$2U' = \alpha \int \left[p^2(\Omega) - < p >^2\right] d\Omega + \beta \int \left[f_{ij}(\Omega) - < f_{ij} >\right]\left[f_{ij}(\Omega) - < f_{ij} >\right] d\Omega$$

…(2.2.25)

where $p(\Omega)\delta_{ij}$ and $f_{ij}(\Omega)$ are the isotropic and deviatoric parts of $p_{ij}(\Omega)$ and

$$\alpha = -\frac{3}{3K_0 + 4G_0}$$

$$\beta = -\frac{3(K_0 + 2G_0)}{5G_0(3K_0 + 4G_0)}$$

where K_0 and G_0 are components of C^0_{ijkl}. (2.2.25) is substituted into (2.2.24) which expresses U_p in terms of U_0 and an integral involving the polarization components. When R_{ijkl} is positive definite,

$$U_p < U$$

when R_{ijkl} is negative definite,

$$U_p > U$$

These two conditions will become bounds on K^* and G^* in terms of polarization components. The variation of U_p is equated to zero and using the relations in (2.2.25), the extremum condition is obtained to be

$$H_{ijkl}(\Omega)p_{kl}(\Omega) - \left[\alpha\delta_{kl}\delta_{ij} + \beta I_{ijkl}\right]\left[p_{kl}(\Omega) - < p_{kl} >\right] = \varepsilon_{ij}^0 \quad (2.2.26)$$

when (2.2.26) is introduced into the equation for U_p, we obtain

$$U_p = U_0 + \frac{1}{2} < \bar{p}_{ij} > \varepsilon_{ij}^0$$

where $\bar{p}_{ij}$ are the polarization components that satisfy (2.2.26).

The elastic modulii of a cubic crystal are completely specified by C_{11}, C_{12}, and C_{44}. The bulk modulii and the two shear modulii of such a crystal are defined by

$$K = \frac{1}{3}(C_{11} + 2C_{12}),$$
$$G_1 = \frac{1}{2}(C_{11} - C_{12}),$$
$$G_2 = C_{44}$$

Since we are considering the Shear Modulus, the ε_{ij}^0 is taken in the deviatoric form and will be denoted by e_{ij}^0 where $e_{kk}^0 = 0$.

Taking the orientation average of (2.2.26) yields the result

$$< H_{ijkl}\bar{p}_{kl} >= e_{ij}^0$$

$$\Rightarrow \frac{1}{3} H_{mmkl} \overline{p}_{kl} \delta_{ij} = e^0_{ij}$$

Taking into account the cubic symmetry and that $e^0_{kk} = 0$, we get

$$\overline{p}_{kk} = 0$$

Hence, the polarization tensor is also deviatoric. On using the above equation, (2.2.26) reduces to

$$\left(H_{ijkl} - \beta I_{ijkl}\right)\overline{p}_{kl} = e^0_{ij} - \beta I_{ijkl} < \overline{p}_{kl} >$$

$$\Rightarrow \overline{p}_{ij}(\Omega) = B_{ijmn}(\Omega)\left(e^0_{mn} - \beta I_{mnkl} < \overline{p}_{kl} >\right) \qquad (2.2.27)$$

where

$A_{ijkl} = H_{ijkl} - \beta I_{ijkl}$

$B_{ijmn} A_{mnkl} = I_{ijkl}$

Averaging both sides of (2.2.27), we get

$$< \overline{p}_{ij} >=< B_{ijmn} > \left(e^0_{nm} - \beta I_{mnkl} < \overline{p}_{kl} >\right)$$

The C_{ijkl} in this case are cubic and the C^0_{ijkl} are isotropic and hence cubic. Thus, H_{ijkl} and B_{ijkl} are also cubic and are given by the three components

$$B_{11} = \frac{H_{11} + H_{12} - \beta}{\left(H_{11} + 2H_{12} - \beta\right)\left(H_{11} - H_{12} - \beta\right)}$$

$$B_{12} = -\frac{H_{12}}{\left(H_{11} + 2H_{12} - \beta\right)\left(H_{11} - H_{12} - \beta\right)}$$

$$B_{44} = \frac{1}{(H_{44} - \beta)}$$

Since B_{ijkl} obeys the elastic modulii symmetry rules, its average can be given in the simplified form as

$$< B_{ijkl} >= B_1 \delta_{ij} \delta_{kl} + 2B_2 I_{ijkl}$$

B_1 and B_2 are found to be

$$B_1 = \frac{1}{5}(B_{11} + 4B_{12} - 2B_{44})$$

$$B_2 = \frac{1}{5}(B_{11} - B_{12} + 3B_{44})$$

Also, we get

$$< \bar{p}_{ij} >= \frac{2B_2}{1 + 2\beta B_2}$$

Introducing this expression into the expression for Up, and applying the extremal conditions, we get

$$G^* \begin{matrix} > \\ < \end{matrix} G_0 + \frac{B_2}{1 + 2\beta B_2} \qquad (2.2.28)$$

The B_2 is expressed in terms of components of C, which gives

$$5B_2 = \left[\frac{1}{2(G_1 - G_0)} - \beta\right]^{-1} + 3\left[\frac{1}{(G_2 - G_0)} - \beta\right]^{-1}$$

This expression when substituted in (2.2.28) yields a monotonically increasing function of K_0 and G_0. Hence, the best lower bound for G^* is obtained for the largest values of K_0 and G_0 i.e. for K and G_1 and the upper bound is obtained for K and G_2. These bounds are obtained to be

$$G_1^* = G_1 + 3\left[\frac{5}{G_2 - G_1} - 4\beta_1\right]^{-1}$$

$$G_2^* = G_2 + 2\left[\frac{5}{G_1 - G_2} - 6\beta_2\right]^{-1}$$

where

$$\beta_1 = -\frac{3(K + 2G_1)}{5G_1(3K + 4G_1)}$$

$$\beta_2 = -\frac{3(K + 2G_2)}{5G_2(3K + 4G_2)}$$

G_1^* and G_2^* provide the bounds for the polycrystalline aggregate. The Voigt-Reuss bounds for a polycrystalline aggregate are given by

$$G_R = \frac{5G_1G_2}{2G_2 + 3G_1}$$

$$G_V = \frac{1}{5}(2G_1 + 3G_2)$$

The material selected is assumed to have cubic symmetry and the constants of Copper are assigned to the material. The C_{11}, C_{12} and C_{44} of Copper are 1.75E11, 1.45E11 and 0.75E11. To induce a slightly greater degree of anisotropy, the C_{44} value is changed to 0.8E11. The bounds are calculated from these constants and are found to be as follows.

Voigt bound = 4.25 GPa

Hashin-Shtrikman lower bound = 4.88 GPa

Hashin-Shtrikman upper bound = 5.24 GPa

Reuss bound = 5.8 GPa

CHAPTER 3

FORMULATION OF THE MINIMAL BOUNDARY CONDITIONS

3.1 The General Linear Elastostatic case

In this section, we develop the formulation for Linear Elastostatics which is the domain of deformation in which the simulations are carried out. This deformation is characterized by a linear relation between the two most important variables of deformation viz. Stress and Strain. The focus here will be to develop the classical strong and weak formulations for a general three-dimensional case.

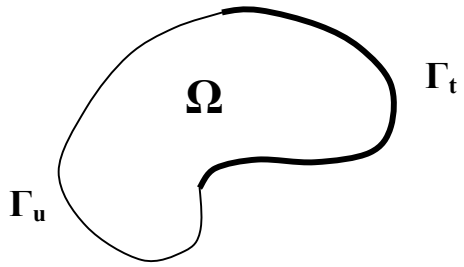

Fig. 3.1 Boundary Conditions for Generalized 3-D Elastostatic case

Ω is defined to be the domain of the body and Γ its boundary. The boundary is divided into two parts,Γ_u where the displacements are prescribed and Γ_t where the tractions are prescribed. Let σ_{ij} denote the Cartesian components of the Cauchy stress tensor, u_i, the components of the displacement vector and f_i be the prescribed body force per unit volume. The strain tensor is defined to be the symmetric part of the displacement gradients given by

$$\varepsilon_{ij} = \frac{u_{i,j} + u_{j,i}}{2} \qquad (3.1.1)$$

The stress and strain tensors are related through the generalized Hooke's law given by

$$\sigma_{ij} = C_{ijkl}\varepsilon_{kl} \qquad (3.1.2)$$

C_{ijkl} are the components of the Constitutive matrix and are also referred to as Elastic coefficients. The matrix **C** is positive definite. These are given functions of **x**. If the elastic coefficients are constant throughout the body, then the body is homogenous. Typically, metals consist of grains in each of which the elastic coefficients are constants. However, from a global perspective, these constants vary with **x** i.e. they do not remain the same for different grains, all of which are represented in a global co-ordinate system. The solution here is the displacement vector **u(x)**.

The strong form of the boundary value problem is given as

Find $u_i \in$ R defined on Ω such that

$$\begin{aligned} &\sigma_{ij,j} + f_i = 0 && \text{in } \Omega \\ &\sigma_{ij} n_j = g_i && \text{on } \Gamma_t \\ &u_i = h_i && \text{on } \Gamma_u \end{aligned} \qquad (3.1.3)$$

The first equation is the equation of equilibrium. **g** and **h** are prescribed functions of traction and displacement on Γ_t and Γ_u respectively. The stress σ_{ij}, is defined in terms of the displacement using the Hooke's law. This Strong form is also referred to as the mixed boundary value problem of elastostatics and possesses a unique solution.

For the Weak formulation of the problem, let S be the trial solution space and V be the variation space. Each of the trial solutions u $\in$ S and the variations w $\in$ V satisfy the prescribed boundary displacement conditions. Multiplying the equilibrium equation with the variation function and integrating it over the domain Ω, we obtain

$$\int_{\Omega} w_i(\sigma_{ij,j} + f_i)d\Omega = 0$$

Integrating by parts, we get

$$-\int_{\Omega} w_{i,j}\sigma_{ij}d\Omega + \int_{\Gamma} w_i\sigma_{ij}n_j d\Gamma + \int_{\Omega} w_i f_i d\Omega = 0$$

In the first integral, σ_{ij} is a symmetric tensor. $w_{i,j}$ is a tensor, which can be expressed as the sum of its symmetric and anti-symmetric parts. The anti-symmetric part of $w_{i,j}$ and σ_{ij} nullify each other which leaves the product of the symmetric part of $w_{i,j}$ and σ_{ij}. Let $w_{(i,j)}$ represent the symmetric part of $w_{i,j}$. w_i is zero on the boundary where the displacements are prescribed (Γ_u), and so the domain of integration of the second integral reduces to Γ_t.

$$-\int_{\Omega} w_{(i,j)}\sigma_{ij}d\Omega + \int_{\Gamma t} w_i g_i d\Gamma_t + \int_{\Omega} w_i f_i d\Omega = 0$$

$$\int_{\Omega} w_{(i,j)}\sigma_{ij}d\Omega = \int_{\Gamma t} w_i g_i d\Gamma_t + \int_{\Omega} w_i f_i d\Omega$$

Thus, the weak form is expressed as

Find $u_i \in S$ and $w_i \in V$ such that, $u_i = h_i$ and $w_i = 0$ on Γ_u and for all $w_i \in V$,

$$\int_{\Omega} w_{(i,j)}\sigma_{ij}d\Omega = \int_{\Gamma t} w_i g_i d\Gamma_t + \int_{\Omega} w_i f_i d\Omega \qquad (3.1.4)$$

3.2 Constraints to be imposed

In the implementation of the minimal boundary conditions, only the strain is imposed over the body. For obtaining a solution, rigid body rotation has to be eliminated. This is done by constraining the displacements of the nodes on the boundary. Consider the body shown in Fig. 3.2.

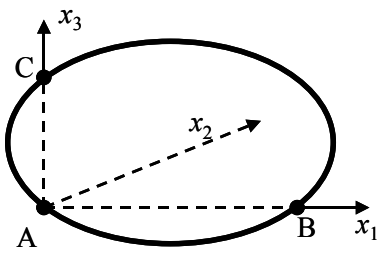

Fig. 3.2 Constraints to prevent rigid Body Rotation for a 3-D case

x_1, x_2 and x_3 are the co-ordinate axes and A, B and C are points on the surface of the body. By imposing displacement constraints in the points A, B and C, rigid body rotation is eliminated. For this, we need six displacements to vanish. These are summed up as

$$\mathbf{u}^A = \mathbf{0}, u_2^B = u_3^B = u_2^C = 0 \qquad (3.2.1)$$

These constraints prevent the rotation of the body about any of the axes.

In the current simulations, a two-dimensional model is used and so the vanishing of six displacements is not required. The constraints required to eliminate rigid body rotation in a two-dimensional case are explained below. Consider the body shown in Fig. 5.3.

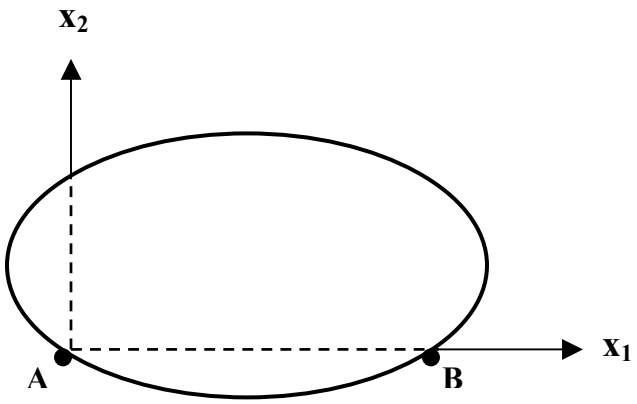

Fig. 3.3 Constraints to prevent rigid Body Rotation for a 2-D case

x_1 and x_2 are the co-ordinate axes and A and B are points on the boundary of the body. The three-dimensional body requires six degrees of freedom to vanish for preventing rigid body rotation. However, for the two-dimensional case, only three

degrees of freedom need to be constrained to prevent rigid body rotation. These constraints are given as

$$\mathbf{u}^A = 0, u_2^B = 0 \tag{3.2.2}$$

It is to be noted that there are only two components of displacement for the point A. These constraints are analogous to the prescribed boundary displacements mentioned in the previous section.

3.3 Formulation of the problem

In this section, the formulation of the problem is developed for the present two-dimensional case with the relevant boundary conditions and constraints. The strong and weak forms are developed for the minimal boundary conditions which impose only the macroscopic shear strain as an average over the area and the constraints mentioned in (3.2.2) for preventing rigid body rotation. The definition for the macroscopic strain is given as the volumetric average of strains over the entire body. This definition, given by Bishop and Hill in 1951, is represented as

$$E_{ij} = \frac{1}{V}\int_V \varepsilon_{ij} dV$$

In the present case, a two-dimensional model is considered. This is represented as

$$E_{ij} = \frac{1}{A}\int_A \varepsilon_{ij} dA$$

$$E_{ij} = \frac{1}{A}\int_A \frac{(u_{i,j} + u_{j,i})}{2} dA$$

$$\Rightarrow \int_A (u_{i,j} + u_{j,i}) dA = 2AE_{ij} = L_{ij}[\mathbf{u}]$$

This, along with the constraints in (3.2.2) is only condition imposed on the body. It should be noted that only the essential boundary conditions are imposed.

The strong form of the boundary value problem is expressed as

Find $u_i \in \mathrm{R}$ defined on Ω such that

$$\sigma_{ij,j} = 0 \qquad \text{in } \Omega$$

$$L_{ij} = 2AE_{ij} \qquad \text{on } \Gamma$$

$$\mathbf{u}^A = \mathbf{0},\ u_2^B = u_3^B = u_2^C = 0$$

Since there are no body forces prescribed, the corresponding term vanishes.

The governing equation for the weak formulation is as given by (3.1.4)

$$\int_\Omega w_{(i,j)}\sigma_{ij}\,d\Omega = \int_{\Gamma t} w_i g_i\,d\Gamma_t + \int_\Omega w_i f_i\,d\Omega$$

Since there are no tractions or body forces, this equation reduces to

$$\int_\Omega w_{(i,j)}\sigma_{ij}\,d\Omega = \int_\Gamma w_i g_i\,d\Gamma$$

Using (3.1.2) and (3.1.1), the above equation can be expressed as

$$\int_\Omega w_{(i,j)} C_{ijkl}\,\frac{(u_{k,l} + u_{l,k})}{2}\,d\Omega = \int_\Gamma w_i g_i\,d\Gamma$$

$$B\left[\mathbf{w}(\mathbf{x}),\ \mathbf{u}(\mathbf{x})\right] = \int_\Gamma w_i g_i\,d\Gamma$$

If there exists a macroscopic stress Σ_{ij}, such that,

$$\Sigma_{ij}\ E_{ij} = \int_\Omega \sigma_{ij}\varepsilon_{ij}\,d\Omega$$

$$\text{then } \Sigma_{ij}\ \delta E_{ij} = \int_\Omega \sigma_{ij}\delta\varepsilon_{ij}\,d\Omega$$

$$\text{But } \int_{\Omega} \sigma_{ij}\delta\varepsilon_{ij}\,d\Omega = \int_{\Gamma} n_j\sigma_{ij}\delta u_i\,d\Gamma$$

$$= \int_{\Gamma} g_i\delta u_i\,d\Gamma$$

One possible solution for **w** is **δu** where **δu** is the virtual displacement. It satisfies all the conditions necessary for **w**. Let us assume the existence of two solutions for **u** viz. **u'** and **u"**. **δu** is defined as

$$\mathbf{\delta u = u' - u"}$$

Since **u'** and **u"** are solutions to the problem, we have

$$\mathbf{u'}^A = \mathbf{u"}^A = \mathbf{0};\ u'^B_2 = u"^B_2 = 0;\ u'^B_3 = u"^B_3 = 0;\ u'^C_2 = u"^C_2 = 0$$

$$\delta\mathbf{u}^A = \mathbf{0},\ \delta u^B_2 = \delta u^B_3 = \delta u^C_2 = 0$$

Also, **u'** and **u"** satisfy

$$L_{ij}[\mathbf{u'}] = L_{ij}[\mathbf{u"}] = 2VE_{ij}$$

Due to the linearity of L_{ij}, this implies

$$L_{ij}[\delta\mathbf{u}] = 0$$

Thus, δ**u** is a solution for **w** and also means that the solution **u** is unique.

Now, $\delta u_i \equiv w_i$ and $\delta E_{ij} \equiv 0$. This means that

$$\sum_{ij} \delta E_{ij} = \int_{\Gamma} g_i\delta u_i\,d\Gamma = \int_{\Gamma} g_i w_i\,d\Gamma = 0$$

Thus the bilinear volume functional vanishes, $B[\mathbf{w}(\mathbf{x}), \mathbf{u}(\mathbf{x})] = 0$

Thus, the weak form of the formulation is given as

Find $\mathbf{u}(\mathbf{x})$ such that $\mathbf{u}^A = \mathbf{0}, u_2^B = u_3^B = u_2^C = 0$ and $L_{ij}[\mathbf{u}] = 2AE_{ij}$, so that for any $\mathbf{w}(\mathbf{x})$, $\mathbf{w}^{\mathbf{A}} = 0$, $w_2{}^B = 0$ and $L_{ij}[\mathbf{w}] = 0$, the bilinear functional vanishes

$$B[\mathbf{w}(\mathbf{x}), \mathbf{u}(\mathbf{x})] = 0$$

The bilinear functional B for the solution $\boldsymbol{\delta}\mathbf{u}$ would be

$$B[\delta\mathbf{u}(\mathbf{x}), \mathbf{u}(\mathbf{x})] = \int_\Omega \delta u_{(i,j)} C_{ijkl} u_{(k,l)}$$

$$= \int_\Omega \delta\varepsilon : \mathbf{C} : \varepsilon \qquad (3.3.1)$$

Due to the symmetry of $\mathbf{C}$, this can be written as

$$\frac{1}{2}\delta\int_\Omega \varepsilon : \mathbf{C} : \varepsilon$$

$$= \frac{1}{2}\delta B[\mathbf{u}(\mathbf{x}), \mathbf{u}(\mathbf{x})]$$

which implies that the problem reduces to minimizing B.

Since the boundary conditions are of an integral nature and the bilinear functional vanishes, the standard weak form is not very helpful in finding the solution. Hence, the method of Lagrange multipliers is adopted.

3.4 Lagrange Multipliers

The problem reduces to minimizing $B[\mathbf{u}(\mathbf{x}), \mathbf{u}(\mathbf{x})]$ subject to $\mathbf{u}^A = \mathbf{0}, u_2^B = u_3^B = u_2^C = 0$ and $L_{ij}[\mathbf{u}] = 2AE_{ij}$.

Upon introducing the Lagrange multiplier λ, for each of the constraints imposed, this can be equivalently stated as minimizing the functional

$$F[\mathbf{u}] = B[\mathbf{u}, \mathbf{u}] - \sum_m \lambda_m \left(L_{ij}[\mathbf{u}] - 2AE_{ij} \right)$$

where *m* is the number of constraints imposed and can vary from 1 to 6. Under variations δu and δλ, such that the allowable variations satisfy $\mathbf{u}^A = 0, u_2^B = u_3^B = u_2^C = 0$, the minimization conditions take the form

$$\delta B[\mathbf{u}, \mathbf{u}] - \sum_m \lambda_m \cdot \delta L_{ij}[\mathbf{u}] = 0 \text{ and}$$

$$\sum_m \delta\lambda_m \cdot \left(L_{ij}[\mathbf{u}] - 2AE_{ij} \right) = 0$$

3.5 Solution Method

Consider a two-dimensional Finite Element mesh with n nodes. Each of the nodes has two degrees of freedom. The total number of degrees of freedom is N which is given by

$$N = 2n$$

Since three degrees of freedom are constrained for the prevention of rigid body rotation, the number of degrees of freedom will be 2N-3. Let p of these degrees of freedom be on the boundary. For the finite element implementation, the minimal boundary condition takes the form

$$\sum_{k=1}^{p} c_k u_k = 2AE_{ij}$$

for each of the constraints imposed. If *m* strains are imposed on the computational model, there would be *m* such equations. The method of expressing the constraint as a summation is elucidated in the next section.

Each of these can be represented in a matrix form as

$$\mathbf{c} \cdot \mathbf{u} = 2AE_{ij}$$

where $\mathbf{c} = \begin{bmatrix} c_1 & c_2 & . & . & c_N \end{bmatrix}$ and $\mathbf{u} = \begin{bmatrix} u_1 \\ u_2 \\ . \\ . \\ u_N \end{bmatrix}$

The different constraints can be expressed in the matrix form shown above. The **u** matrices would be the same for all the constraints, since they represent the displacement of the nodes. The **c** matrices would be different for different constraints.

The minimal boundary conditions can also be expressed as fulfilling the function

$$\mu_m = \mathbf{c}^m \cdot \mathbf{u} - 2AE_{ij} = 0$$

Since there are no prescribed boundary tractions, the Finite Element form of the potential energy is

$$\pi = \frac{1}{2}\mathbf{u}^T\mathbf{K}\mathbf{u}$$

Consider the function

$$F(\mathbf{u}, \lambda) = \pi(\mathbf{u}) - \lambda_m \mu_m(\mathbf{u})$$

where λ_m is a scalar multiplier called the Lagrange Multiplier. Rendering the above equation stationary is equivalent to satisfying the constraint imposed by the minimal boundary condition. The condition of being stationary simplifies to

$$\mathbf{a}^T\left(\mathbf{K} \cdot \mathbf{u} - \sum_m \lambda_m \left(\mathbf{c}^m\right)^T\right) - b\sum_m \left(\mathbf{c}^m \cdot \mathbf{u} - 2AE_{ij}\right) = 0$$

Since **a** and *b* are arbitrarily selected,

$$\mathbf{K} \cdot \mathbf{u} - \lambda_m \left(\mathbf{c}^m\right)^T = 0 \text{ and } \mathbf{c}^m \cdot \mathbf{u} - 2AE_{ij} = 0$$

for each of the *m* macroscopic strain constraints imposed.

This is represented as

$$\sum_{j=1}^{N} K_{ij} u_j - c_i^m \lambda_m = 0 \qquad \text{j = 1,2,3…N}$$

$$\sum_{k=1}^{N} c_k^m u_k = 2AE_{ij}$$

Thus we have $N + m$ unknowns viz. the N degrees of freedom and the m Lagrange multipliers which can be solved using the $N + m$ equations.

The commercial software ABAQUS is used for carrying out the simulations. This software, however, does not use Lagrange multipliers as stated above for a constraint imposed using the *EQUATION option. The solution is obtained by solving for one of the displacements in terms of the other. For e.g.

$$u_1 = \frac{1}{c_1^1}\left[2AE_{ij} - \sum_{i=2}^{N} c_i^1 u_i\right]$$

The homogenous system of equations which is to be solved is given by

$$\sum_{j=1}^{N} K_{ij} u_j = 0 \qquad i = 1,2,3\ldots N$$

$$K_{i1} u_1 + \sum_{j=2}^{N} K_{ij} u_j = 0$$

$$K_{i1} \frac{1}{c_1^1}\left[2AE_{ij} - \sum_{k=2}^{N} c_k^1 u_k\right] + \sum_{j=2}^{N} K_{ij} u_j = 0$$

$$\sum_{j=2}^{N}\left[K_{ij} - K_{i1}\frac{c_j^1}{c_1^1}\right]u_j = -K_{i1}\frac{1}{c_1^1}2AE_{ij} \qquad i = 2,3,\ldots,\mathrm{N}$$

The above equation yields *N*-1 equations with *N*-1 unknowns. This process of expressing one degree of freedom in terms of the remaining is done for each of the constraints imposed. If *m* constraints are imposed, we finally have *N-m* equations with as many unknowns.

3.6 Finite Element Implementation

In this section, the finite element implementation of the minimal boundary conditions for a two-dimensional case is presented. Bishop and Hill (1951) have provided the universal definition for macroscopic strain as the volumetric average of strain of infinitismal volume elements over the entire domain of the body. Analogous definitions have been provided by Gurson (1977) for granular materials. The Bishop and Hill definition is given as

$$E_{ij} = \frac{1}{V}\int_V \varepsilon_{ij}\,dV$$

$$E_{ij} = \frac{1}{V}\int_V \frac{\left(u_{i,j} + u_{j,i}\right)}{2}dV$$

using the Gauss theorem,

$$E_{ij} = \frac{1}{2V}\int_S \left(u_i n_j + u_j n_i\right)dS$$

where S is the boundary of the domain and n is the normal to the boundary. Thus, the minimal boundary conditions can be applied to any shape of the representative volume element as long as the normal to the boundary is known. Also note that the conditions can

be applied incrementally to non-linear problems (du = vdt). This can be done since the formulation is valid irrespective of additional kinematic variables.

For the present two-dimensional case the macroscopic strain is defined over the area and the integral reduces to a boundary integral given by

$$E_{ij} = \frac{1}{2A}\int_S (u_i n_j + u_j n_i)\,dS$$

The test case here is a linear elastic problem where only shear strain is imposed. Hence the equation takes the form

$$E_{12} = \frac{1}{2A}\int_S (u_1 n_2 + u_2 n_1)\,dS$$

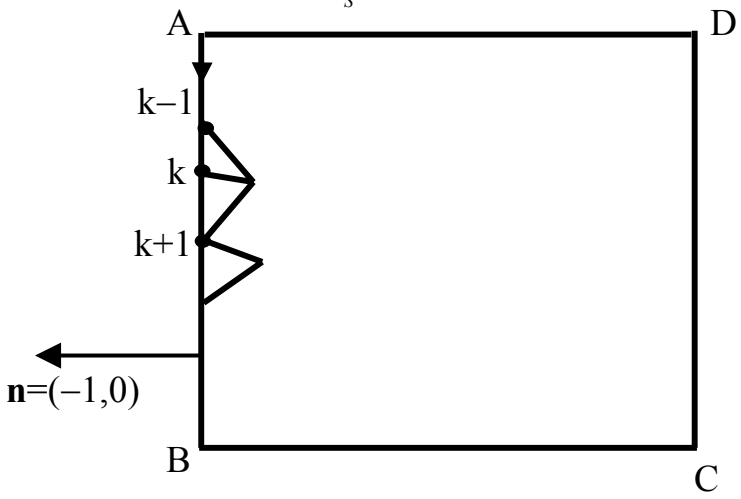

Fig. 3.4 Schematic of the case for which the Boundary Conditions are implemented

Shown above is a schematic of the two-dimensional domain on which the minimal boundary conditions will be imposed. AB, BC, CD and DA constitute the boundary (S) of the domain. The integral in reduces to

$$2AE_{12} = \int_A^B (u_1 n_2 + u_2 n_1)\,dS + \int_B^C (u_1 n_2 + u_2 n_1)\,dS + \int_C^D (u_1 n_2 + u_2 n_1)\,dS + \int_D^A (u_1 n_2 + u_2 n_1)\,dS$$

The normal (n), is shown for the side AB in the figure. The magnitude of the y-component of the normal is 0. For each of the sides of the boundary, one component of the normal is 0. Thus, the equation reduces to

$$2AE_{12} = -\int_A^B u_2 dS - \int_B^C u_1 dS + \int_C^D u_2 dS + \int_D^A u_1 dS$$

The integral $\int_A^B u_2 dS$ can be expressed as a summation of the product of the displacement of a node and its weight function. This can be represented as

$$\int_A^B u_2 dS = \sum_k u_2^k \int_A^B \psi_k dS$$

where $\int_A^B \psi_k dS$ is referred to as the weight of the node k. In a rough sense, it is the importance of the node k in the finite element mesh. In the current case, constant strain elements are used. The weight of the node k is the area of the triangle formed by it with its two adjacent nodes as the base and a height of 1. This is demonstrated in the figure.

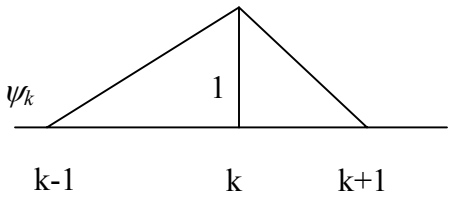

Fig. 3.5 Calculation of Weight Functions for Constant Strain Elements

Thus, the integral in changes to a summation of the products of the displacements of the nodes and their corresponding weight functions. Let there be p number of nodes on the boundary. The minimal boundary condition is expressed as

$$\sum_{i=1}^{p} c_i u_i = 2AE_{12}$$

CHAPTER 4

MODELING AND SIMULATIONS

The objective of the current research is to analyze the response of a heterogeneous material to an externally imposed strain. Metals, when considered at a small length scale can be considered to be heterogeneous. At a larger length scale, however, metals are approximated and assumed to be isotropic and homogeneous.

Metals are composed of grains or crystals. Each grain has a specific orientation in which their physical constants are expressed. The orientation differs from one grain to another. The physical constants of all the grains are the same when they are expressed in the direction in which the grain is orientated. However, when the physical constants are expressed in a global co-ordinate system, which remains fixed, the values of the constants change from one grain to another. Thus, the two most important aspects of modeling are the determination of the shape of the grains, their dimensions etc. and the directions in which they are oriented. The simulations are carried out using the commercial Finite Element software ABAQUS. The issue of shape and size of the grains is addressed first here.

4.1 Modeling the Microstructure

The assembly of grains required for the simulations is generated using Voronoi Tessellation. Voronoi Tessellation is one of the most commonly used methods for the generation of microstructure. It provides a reasonably good representation of the microstructure, albeit with some approximations.

The concept of voronoi tessellation is to mimic the growth of grains as a metal solidifies assuming that the temperature gradients are very small in the solidifying regime. Since the temperature gradients are assumed to be very small, a number of crystals start forming at the same instant of time. The points of origin of solidifications are called seed points and occur randomly in space. Also, all the crystals grow at the same rate in all directions due to the uniform temperature. The crystals keep growing until the growth is opposed by the growth of the neighboring crystals. A grain boundary forms at the space where the two crystals oppose each other.

Since all the crystals grow at the same rate, the grain boundary between two seed points is a plane which is normal to the line joining the two seed points and passes through the mid-point of this line. In a two-dimensional case, the grain boundary is the perpendicular bisector of the line joining the seed points. Numerous such seed points lead to the formation of closed polygons (grains), each corresponding to a seed point. The important fact to be realized is that every point in such a closed polygon is closest to the seed point of that polygon than to any other seed point.

The voronoi tessellation for the present case is performed using the commercial software MATLAB. The size of the grains depends on the relative positioning of the seed points i.e. the farther the seed points, the larger the size of the grain. To prevent large differences in the sizes of the grains, the seed points are generated such that uniformity in size is maintained.

The process of generation of the seed points for this purpose is simple, yet very effective. The domain of the model is divided into as many number of squares of uniform

area as the number of grains to be modeled. A seed point is generated in each of these squares of uniform area. The process of generation of the co-ordinates of the seed point is randomized i.e. the x co-ordinate of the seed point for a square is a random number whose value lies between the extremities of the square. The y co-ordinate is also generated through the same process. Thus, a random point is generated in each of the squares in the domain.

The co-ordinates of these randomly generated points are input into MATLAB which generates a voronoi diagram with these points as the seed points. MATLAB also provides the vertices of the polygons generated. These polygons are recreated in ABAQUS using the co-ordinates of the vertices. The grains are assembled as in the voronoi diagram which creates a computational model of the microstructure.

The simulations are carried out in the linear elastic regime of the deformation of materials. In this regime of deformation, there is no sliding or cleavage at the grain boundary. So, the edges of each polygon (grain boundary) are rigidly tied with the corresponding edges of the adjacent polygons (grains). Triangular, constant strain, Plane strain elements are used for the meshing of the assembly. Grain boundaries have the same number of nodes on the boundary corresponding to each grain so that continuity of displacements in maintained.

Since the grains are anisotropic, the deformation, even though elastic, produces substantial variations of stress in a single grain. These variations are effectively represented by the large number of elements in each grain. The 25 grain assembly has an average of 53 elements per grain, the 100 grains assembly, 56 per grain and the 400

grains assembly has an average of 58 elements per grain. The assembly for 25 grains is shown with a sample finite element mesh of one of the grains.

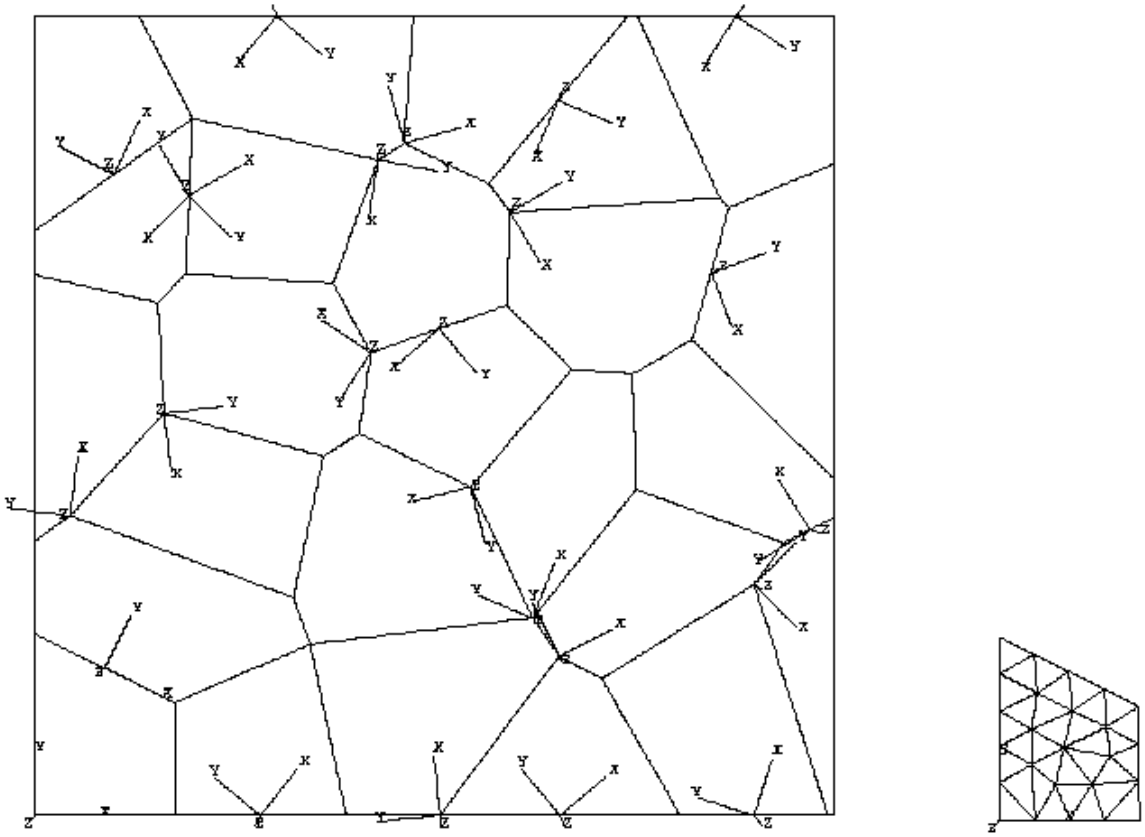

Fig. 4.1 Assembly of 25 grains and Finite Element Mesh of one grain

4.2 Modeling the Material

A solid body changes its shape when subjected to an external force or stress. For sufficiently small amounts of stress, the strain is linearly proportional to the magnitude of stress. The constitutive relation is called the Hooke's law and is expressed as

$$\sigma_{ij} = C_{ijkl}\varepsilon_{kl}$$

where C is the stiffness tensor.

It can be observed that the stiffness tensor has 81 components corresponding to the four indices. However, due to symmetry of the stress and strain tensors, there are a maximum of 21 independent constants in the stiffness tensor. For convenience, the constitutive relation is now expressed as

$$\sigma_i = C_{ij}\varepsilon_j$$

where the stress and strain are column matrices and C is a 6X6 symmetric matrix.

There are a maximum of 21 independent constants in the C matrix. However, this number reduces with the nature of the material and the symmetries inherent to the material. In the present case, a material with cubic symmetry is considered which reduces the number of independent components of C to three. This is shown below

$$C = \begin{pmatrix} c_{11} & c_{12} & c_{12} & . & . & . \\ & c_{11} & c_{12} & . & . & . \\ & & c_{11} & . & . & . \\ & & & c_{44} & . & . \\ & & & & c_{44} & . \\ & & & & & c_{44} \end{pmatrix}$$

These constants are however, subject to the conditions

$$c_{11} > |c_{12}|,\ c_{11} + 2c_{12} > 0,\ c_{44} > 0$$

The material used for the simulations is Copper. However, the values of the elastic constants have been slightly altered to induce greater anisotropy.

In the current model, each grain of the assembly is oriented differently. ABAQUS requires the upper triangular C matrix to be input to define the properties of the material. This can be done by defining the orientation of each grain in which the stiffness matrix is defined. However, in such a case, the output variables viz. stress etc. are also given in the

same orientation instead of the global orientation. To overcome this problem, the stiffness matrix is transformed into the desired orientation and the constants are expressed in a global co-ordinate system.

The transformation is done through a homemade FORTRAN code. It is to be noted that the elastic constants cannot be transformed as a matrix, but have to transformed as a fourth order tensor. The constants of the matrix are plugged back as components of the fourth order stiffness tensor and transformed as a tensor given by

$$C'_{ijkl} = a_{im} a_{jn} a_{ko} a_{lp} C_{mnop}$$

where the **a** matrices are the directional cosine matrices for transformation.

The constants corresponding to the upper triangular C matrix are extracted back and input into ABAQUS. Thus, the grain behaves as if it is oriented in a specified direction, but all the variables are now expressed in the global co-ordinate system. Each orientation requires a different directional cosine matrix and consequently yields different values for the elastic constants. This means for every grain and its corresponding orientation, a new material has to be defined which has its own set of constants. Thus, as many number of different materials are defined as the number of grains.

4.3 Orientations

The material being modeled has cubic symmetry. Thus, only orientations from $-\pi/4$ radians to $\pi/4$ radians with respect to the global axes are independent. Any other orientation yields the same constitutive matrix as one of the orientations from $-\pi/4$ to $\pi/4$ radians. So, the orientations assigned to the materials are selected from the domain $[-\pi/4, \pi/4]$. Orientations are assigned using two methods viz. uniform probability

distribution and enforced uniform distribution. Five realizations of orientations are simulated for each of the assemblies for each of the boundary conditions.

4.3.1 Uniform Probability Distribution

As the title suggests, every orientation assigned to the grains has an equal probability of being selected. The domain of possible orientations is $[-\pi/4, \pi/4]$ radians. Random numbers are generated in the domain [-1,1] and are multiplied with $\pi/4$ which gives the orientation of a particular grain with respect to the global axes. All the random numbers are generated independent of each other i.e. the random numbers generated till a particular point of time have no impact on the number which is generated next. Thus, every orientation has an equal probability of being selected and this method is hence termed Uniform Probability Distribution.

4.3.2 Enforced Uniform Distribution

In this method, orientations assigned to grains are selected randomly from uniformly spaced intervals in the domain of orientations. The domain of orientations $[-\pi/4, \pi/4]$ is divided into equal intervals. The number of intervals is equal to the number of grains. A random number is generated in each of these intervals and is randomly assigned to a grain. Once an orientation has been selected from an interval, it is discarded and so is the grain to which the orientation has been assigned, the idea being orientations throughout the entire spectrum $[-\pi/4, \pi/4]$ have to be encompassed in a finite number of grains.

Both these methods of assigning orientations are repeated to obtain five sets of orientations for the assembly of the grains. The process of selecting an orientation and

assigning to a grain is randomized and is accomplished using a homemade FORTRAN code. The code uses four different randomly generated sequences of numbers to select an orientation and assign it to a grain.

4.4 Boundary Conditions

The assembly so created, is subjected to different boundary conditions with the same macroscopic shear strain being imposed in each case. Three different boundary conditions are imposed on the assembly viz. Rigid Boundary Conditions, Periodic Boundary Conditions and Minimal Boundary Conditions.

4.4.1 Rigid Boundary Conditions

These boundary conditions impose rigidity of the boundary along with periodicity. The boundary does not have the freedom to change its shape i.e. a straight remains straight. This is illustrated in Fig. 1.2 (a).

This boundary condition is simulated by prescribing the corresponding displacements of all the nodes that lie on the boundary. The boundary at the base of the assembly is completely fixed. No node on any boundary has vertical displacement.

4.4.2 Periodic Boundary Conditions

Periodic boundary conditions do not impose rigidity of the boundary, but they impose periodicity of the unit cell. Periodic boundary conditions impose that opposite sides of the unit cell deform parallel to each other. If many of such deformed unit cells were taken, they would fit each other along the boundary since they deform in a parallel manner. This is illustrated in Fig. 1.2 (b).

The assembly is constrained so that rigid body rotation is prevented. The condition that opposite sides have to deform parallel to each other is achieved by specifying that the displacements of the nodes on opposite boundaries have to be the same. If an imaginary co-ordinate system is placed at the center of the assembly and L gives the dimension of the assembly, the Periodic boundary conditions are stated in equation form as

$$\underline{\mathbf{u}}\left(x_1, \frac{L}{2}\right) = \underline{\mathbf{u}}\left(x_1, \frac{-L}{2}\right)$$
$$\underline{\mathbf{u}}\left(\frac{L}{2}, x_2\right) = \underline{\mathbf{u}}\left(\frac{-L}{2}, x_2\right)$$

If the nodes do not have the same co-ordinates, the displacement is prescribed as a linear interpolation of the nearest nodes on the opposite boundary. The displacements of the nodes are related using the *EQUATION keyword in ABAQUS.

4.4.3 Minimal Boundary Conditions

The Minimal boundary conditions are the conditions which impose the least constraints on the material and hence the name “Minimal” boundary conditions. These boundary conditions do not impose rigidity or periodicity at the boundary. The only constraint imposed is the macroscopic shear strain as the average of the strains over the entire area. The formulation of the constraints has been demonstrated in the previous chapter. The constraint is expressed as the summation of products of the displacements of nodes and their weight functions over the boundary of the domain. This is given by

$$\sum_{i=1}^{N} c_i u_i = 2AE_{mn}$$

The constraint is imposed using the *EQUATION keyword in ABAQUS.

4.5 Shear Modulus

The different boundary conditions are imposed on the assembly to deform it. Stresses develop in the material due to the strain imposed in the form of displacements on the boundary. Due to the different orientations for different grains, the stresses developed in each grain are different. Since constant strain elements are used, the stresses in each element are constant. To calculate the average response of the material, the average shear modulus over the entire assembly is calculated using a homemade FORTRAN code.

The average shear modulus is defined to be the ratio of the average shear stress to the average shear strain. The average shear stress is calculated as the weighted average of the stresses of the elements. The nodes forming an element and the co-ordinates of the nodes are read from the ABAQUS input file from which the area of the element is calculated. The corresponding shear stress of the element is extracted from the output data file of ABAQUS. The shear stress in the element is multiplied with the area of the element. This operation is performed over all the elements and the products are summed up. The ratio of this sum to the total area gives the weighted average of the shear stress over the entire area. The ratio of this average stress to the imposed macroscopic strain gives the shear modulus of the assembly.

The deformation simulations are repeated for five sets of uniform probability distribution and five sets of enforced uniform distribution. The values of the shear modulus are expected to lie between the bounds derived in chapter 2.

CHAPTER 5

FOURIER TRANSFORMS OF THE FIELD VARIABLES

5.1 Fourier Transform

A principal analysis tool in many of today's scientific applications is the Fourier Transform. Possibly, the most well known application of this mathematical technique is the analysis of linear time-invariant systems. But, the Fourier transform is essentially a universal problem-solving technique. Its importance is based on the fact that one can examine a particular relationship from an entirely different point of view. Simultaneous visualization of a function and its Fourier transform is often the key to successful problem solving.

The essence of the Fourier transform of a waveform is to decompose or separate the waveform into a sum of sinusoids of different frequencies. If these sinusoids sum to the original waveform, we have determined the Fourier transform of the waveform. The Fourier transform identifies or distinguishes the different frequency sinusoids, and their respective amplitudes, that combine to form the arbitrary waveform. Mathematically, the relationship is stated as

$$S(f) = \int_{-\infty}^{\infty} s(t) e^{-i2\pi ft} dt \tag{5.1.1}$$

where *s(t)* is the waveform to be decomposed into a sum of sinusoids, *S(f)* is the Fourier transform of *s(t)*, and i = √-1. Typically, *s(t)* is termed a function of the variable time and *S(f)* is termed a function of the variable frequency.

In general, the Fourier transform is a complex quantity:

$$S(f) = R(f) + I(f) = |S(f)|e^{i\theta(f)}$$

where *R(f)* is the real part of the Fourier transform,

I(f) is the imaginary part of the Fourier transform,

$|S(f)|$ is the amplitude of the Fourier spectrum of *s(t)* given by $\sqrt{R^2(f) + I^2(f)}$,

$\theta(f)$ is the phase angle of the Fourier transform given by $\tan^{-1}[I(f)/R(f)]$.

If the waveform *s(t)* is not periodic, then the Fourier transform will be a continuous function of frequency, that is, *s(t)* is represented by the summation of sinusoids of all frequencies. The Fourier transform is a frequency-domain (inverse of wavelength) representation of a function. The Fourier transform frequency domain contains exactly the same information as that of the original function, albeit they differ in their manner of representation.

5.2 Discrete Fourier Transform

The Fourier transform is defined for continuous functions. However, Fourier transforms of functions can also be obtained through sampling of the function at regular time intervals which forms the basis for Discrete Fourier transforms and Fast Fourier transforms. Clearly, Discrete Fourier transforms can be derived independently of the Fourier integral. However, it can be demonstrated that Discrete Fourier transforms are actually a special case of the Fourier integral.

The Discrete Fourier transform is of interest primarily because it approximates the Continuous Fourier transform. Validity of this approximation is strictly a function of the waveform being analyzed. The differences in the two transforms arise because of the

Discrete transform requirement of sampling and truncation. However many of the scientific applications of the Continuous Fourier transforms rely on a digital computer for implementation, which leads to the direct use of the Discrete Fourier transform and hence the Fast Fourier transform.

The Discrete and Fast Fourier transforms are certainly ubiquitous because of the great variety of apparently unrelated fields of application. However, the proliferation of applications across broad and diverse areas is because they are united by a common entity, The Fourier Transform. FFTs and DFTs find applications in structural dynamics, acoustics, signal processing, radar technology, communications and a host of other areas.

The terms of the Discrete Fourier transform are given as

$$H\left(\frac{n}{NT}\right) = \sum_{k=0}^{N-1} h(kT)e^{-i2\pi nk/N} \qquad n = 0,1,2,\ldots,N\text{-}1 \qquad (5.2.1)$$

where N is the total number of sampling points and T is the time period between two successive sampling points, $h(kT)$ is the value of the function at point kT and H is the Fourier transform of the function h. It is of primary importance that there are enough number of sampling points that can represent the properties of the function being sampled.

Similarly, the two-dimensional Fourier transform is given by

$$H\left(\frac{n}{NT_x},\frac{m}{MT_y}\right) = \sum_{q=0}^{M-1}\left[\sum_{p=0}^{N-1} h(pT_x,qT_y)e^{-i2\pi mp/N}\right]e^{-i2\pi mq/M} \qquad (5.2.2)$$

where n = 0,1,2,…,N-1 and m = 0,1,2,…,M-1. N and M are the number of sampling points taken in x and y directions and T_x and T_y are the respective time periods of

sampling points. *h* is an m x n matrix which represents the functional values and *H* is the Fourier transform of *h* which is also an m x n matrix.

From the above equation, it can be noted that a one-dimensional Fourier transform is carried out for each column and row wise Fourier transformation is carried out for these transformed columns. The total number of computations required for the two-dimensional transform is immense. For an m x n matrix, it requires m^2n^2 multiplications of complex numbers and a huge number of additions of complex numbers to arrive at the final Fourier transform. If we consider an n x n square array, the number of multiplications of complex numbers required is n^4 and we also need to perform $n^2(n-1)^2$ complex additions. Cooley and Turkey proposed a mathematical algorithm in 1965 which reduces the computational time to be proportional to $n^2\log_2 n$. This algorithm is widely recognized as the "Fast Fourier Transform".

5.3 Present Methodology

The Fourier transform can be interpreted as the mapping of a function to a frequency domain i.e. the dependence of the function for a particular frequency. From (5.2.1), it can be seen that transform gives the dependence on frequencies given by *n/NT*.

This means the terms correspond to a wavelength of *NT/n*. (5.3.1)

The amplitude of the term gives the dependence of the function or the significance of that particular wavelength.

In the current context, Fourier transforms of the deviations of stress from the average stress are performed. The stress values for the transform are obtained using a homemade code. The code generates a grid of points in each of the assemblies created.

The grain in which a particular point lies is determined. The code then forms triangles with the current point and two nodes of each element in the grain at a time for all the nodes. Thus, three triangles are formed for each element in the grain with the given point. The areas of these three triangles are found out and so is the area of the triangular element. If the sum of the areas of the three triangles formed by the point and the nodes of an element is equal to the area of the element, then the given point lies inside that particular element. If not the code proceeds to perform the same check on the next element of that grain. The code goes through all the elements of a grain irrespective of whether previously an element had been obtained in which the point lies. This is because the point might be co-incident with a node of an element or might lie on the side of an element, in which cases, all the elements in which the point lies are stored. The stresses of all the elements in which the point lies are extracted and are averaged. This gives the stress value at that point. If the point lies solely in one element, the stress in that element is the stress value at the point.

This computation is repeated for the entire grid of points and the stress values of all the points are stored in a matrix. The average of the values of all the elements in this matrix gives the average stress value for the grid of points. This average value is subtracted from each element of the matrix. This gives a matrix of the deviation from the average stress of the grid of points. A two-dimensional FFT of this matrix gives the dependence of the deviations of the stress from the average for different frequencies and their corresponding wavelengths.

Since the FFT is performed for the deviations of stress from the average, the output indicates the periodicity and dependence of stress variations for various length scales of the domain. The domain here is a polycrystalline aggregate and so the length scales can be associated with the size of the grains consisting the domain. The grains of the assembly are each oriented differently and so have different stresses in them. Hence, the stress varies at each grain boundary. Thus, we expect to see a strong dependence of the FFTs for a length scale corresponding to one grain and integral multiples of a grain.

From (5.3.1), we know that the terms of the Fourier Transform correspond to a wavelength of NT/n where $n = 0, 1, 2\ldots N\text{-}1$. N is the number of sampling points and T is the time period of sampling. If l is the length of the domain, then

$$T = \frac{l}{N-1} \tag{5.3.2}$$

the wavelength corresponding to the term n, denoted by λ_n is given by

$$\lambda_n = \frac{Nl}{(N-1)n} \qquad n = 0,1,2\ldots N\text{-}1 \tag{5.3.3}$$

For the 5 x 5 grain assembly, a grid of 10,000 points is formed i.e. $N = 100$.

The wavelengths are given as

$$\lambda_n = \frac{100l}{99n} \qquad n = 0,1,2\ldots \text{N-}1 \tag{5.3.4}$$

for $n = 0$, the wavelength is $\lambda_0 = \infty$. The successive wavelengths are $\lambda_1 = \frac{100}{99} \times \frac{l}{1}$,

$\lambda_2 = \frac{100}{99} \times \frac{l}{2}$, $\lambda_3 = \frac{100}{99} \times \frac{l}{3}$ and so on.

The 10 x 10 assembly has a sample size of 150 points. The wavelengths are given by

$$\lambda_n = \frac{150l}{149n} \qquad n = 0,1,2\ldots N\text{-}1 \qquad (5.3.5)$$

for $n = 0$, the wavelength is $\lambda_0 = \infty$. The successive wavelengths are $\lambda_1 = \frac{150}{149} \times \frac{l}{1}$,

$\lambda_2 = \frac{150}{149} \times \frac{l}{2}$, $\lambda_3 = \frac{150}{149} \times \frac{l}{3}$ and so on.

The 20 x 20 assembly has a sample size of 200 points. The wavelengths are given by

$$\lambda_n = \frac{200l}{199n} \qquad n = 0,1,2\ldots N\text{-}1 \qquad (5.3.6)$$

for $n = 0$, the wavelength is $\lambda_0 = \infty$. The successive wavelengths are $\lambda_1 = \frac{200}{199} \times \frac{l}{1}$,

$\lambda_2 = \frac{200}{199} \times \frac{l}{2}$, $\lambda_3 = \frac{200}{199} \times \frac{l}{3}$ and so on.

The input for the FFTs is in the form of an array. This array is uploaded into MATLAB and the two dimensional FFT is performed. This results in an array of equal dimensions of the input. However, the terms of the output array are amplitudes of the corresponding frequencies. As demonstrated above, each term of the FFT represents a particular wavelength or a specific length spectrum of the domain. The wavelength decreases as the terms of the FFT progress and we soon arrive at wavelengths which are smaller than the size of a grain. These wavelengths are insignificant and are eliminated. The terms of the FFT whose wavelengths are significant are selected and a smooth surface is fitted through them using cubic interpolation in MATLAB. The resultant surface is smooth which renders the peaks more visible and also projects the significance of intermediate wavelengths.

5.4 Aliasing

The accuracy of the Discrete Fourier transform does depend on the number of sampling points. The frequency of sampling has to be equal to or greater than the largest frequency of the sampled function. Sampling lesser number of points results in a distorted FFT. This phenomenon is known “Aliasing”.

The sampled function is the variation of stresses from the average. Since constant strain elements are used, the elements have constant stresses. Thus, the largest frequency of stress variation is from an element to element. So, the number of sampling points has to be greater than the number of elements. This criterion is fulfilled many times over in all the cases.

CHAPTER 6

RESULTS AND DISCUSSION

The assemblies of grains created are subjected to the various boundary conditions and the simulations are performed for different realizations of orientations. The overall response of the crystalline aggregate, the stress distributions and the effectiveness of the minimal boundary conditions are discussed here.

6.1 Overall Elastic Response of the Crystalline Aggregate

The deformation of the crystalline aggregate is simulated using the different boundary conditions. The overall elastic shear stress is calculated using a weighted average of the stresses in each element of the finite element mesh. The average shear modulus of the aggregate, which is the ratio of the weighted average stress to the macroscopic strain, for Uniform Probability Distribution of orientations is shown in the tables below for different sizes of the RVE.

	Orientation 1	**Orientation 2**	**Orientation 3**	**Orientation 4**	**Orientation 5**
Rigid	5.321	5.8741	5.4509	6.0312	5.5247
Periodic	5.1258	5.606	5.0051	5.7028	5.104
Minimal	4.4156	4.7733	4.559	5.3013	4.6313

Table 6.1 Shear Modulus (in GPa) for 25 Grains assembly

	Orientation 1	**Orientation 2**	**Orientation 3**	**Orientation 4**	**Orientation 5**
Rigid	5.3797	5.9438	5.475	5.1595	5.2957
Periodic	5.1622	5.7339	5.2962	4.9744	5.0551
Minimal	4.6936	5.3626	4.9318	4.5364	4.6935

Table 6.2 Shear modulus (in GPa) for 100 grains assembly

	Orientation 1	Orientation 2	Orientation 3	Orientation 4	Orientation 5
Rigid	5.3036	5.4753	5.4025	5.3864	5.5708
Periodic	5.2079	5.3808	5.253	5.2479	5.4591
Minimal	5.0725	5.2185	5.0851	5.0684	5.3359

Table 6.3 Shear modulus (in GPa) for 400 grains assembly

The average shear modulus, which indicates the stiffness of the material, shows that the Rigid boundary conditions impose the stiffest constraints on the body followed by Periodic and Minimal boundary conditions respectively. This is due to the fact that Rigid conditions impose rigidity with periodicity. For every simulation, the Minimal boundary conditions impose the least constraints which indicates that the body deforms more relaxedly as expected i.e. for every orientation, the shear modulus for the Minimal boundary conditions is lower than those for Rigid and Periodic boundary conditions.

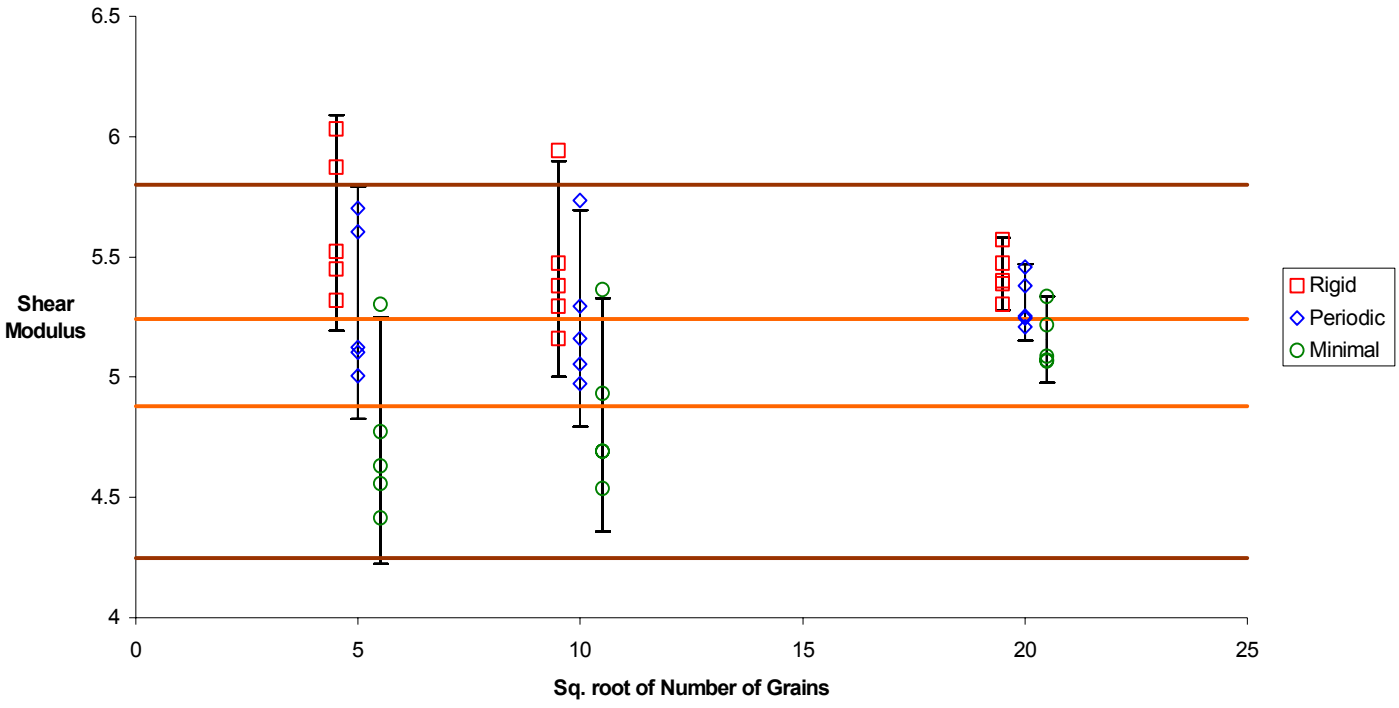

Fig. 6.1 Shear Modulii for different realizations of Uniform Probability Distribution

The above graph shows the response of the aggregate for various sizes of the RVE. The ineffectiveness of the Rigid and Periodic boundary conditions and the superiority of the Minimal boundary conditions is evident. The Rigid and Periodic boundary conditions are very stiff even for the assembly of 100 grains. The minimal boundary conditions give more freedom for the body to deform. For the RVE of 400 grains, the minimal boundary conditions are comprehensively better than the other two with almost all the responses lying in the Hashin-Shtrikman bounds.

The overall responses for Enforced Uniform Distribution are presented below.

	Orientation 1	**Orientation 2**	**Orientation 3**	**Orientation 4**	**Orientation 5**
Rigid	5.8005	5.719	5.3655	5.7203	5.8485
Periodic	5.6057	5.22	5.1325	5.2238	5.2811
Minimal	4.7378	4.9317	4.7068	4.7801	4.669

Table 6.4 Shear Modulus (in GPa) for 25 Grains assembly.

	Orientation 1	**Orientation 2**	**Orientation 3**	**Orientation 4**	**Orientation 5**
Rigid	5.5131	5.4796	5.5286	5.4825	5.5838
Periodic	5.3387	5.2859	5.276	5.2944	5.3339
Minimal	4.9957	4.9253	4.9249	4.9707	5.0114

Table 6.5 Shear modulus (in GPa) for 100 grains assembly

	Orientation 1	**Orientation 2**	**Orientation 3**	**Orientation 4**	**Orientation 5**
Rigid	5.3925	5.4623	5.4832	5.4309	5.4897
Periodic	5.2488	5.3574	5.4008	5.2806	5.3721
Minimal	5.1153	5.2367	5.2202	5.1597	5.208

Table 6.6 Shear modulus (in GPa) for 400 grains assembly

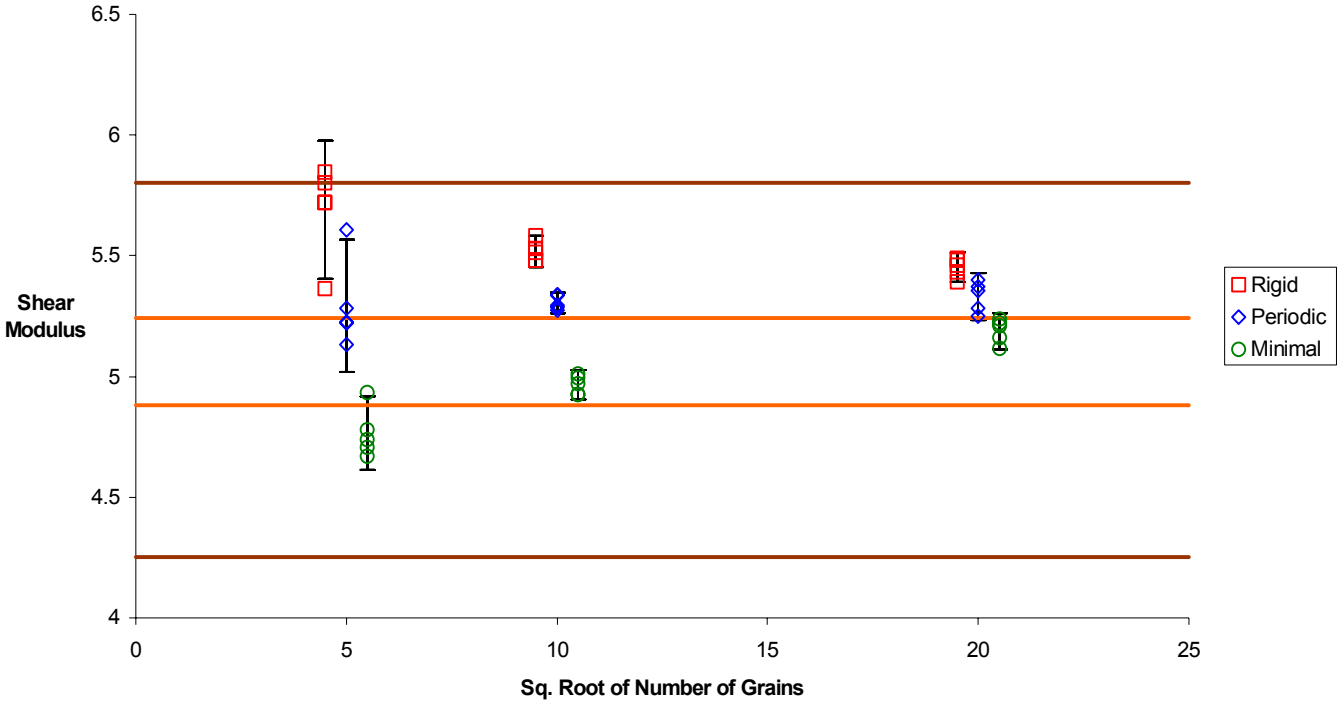

Fig. 6.2 Shear Modulii for different realizations of Enforced Uniform Distribution

The trend observed for the uniformed probability distribution continues with the enforced uniform distribution. The average shear modulus for the Rigid Boundary Conditions are highest followed by the Periodic boundary conditions and then by the Minimal boundary conditions. However, the effect is more pronounced because the orientations assigned to the grains are uniformly distributed throughout the domain of orientations.

An RVE size of 100 grains gives perfect results, all the responses lying in the Hashin-Shtrikman bounds. Also, the range over which the shear modulii are spread for each boundary condition decreases with the increase of the RVE size. The responses for different boundary conditions also come closer to each other indicating that as the RVE

size tends towards infinity, there would be no difference between the three boundary conditions.

The Hashin-Shtrikman bounds and the Voigt-Reuss bounds have been derived for an infinite assembly of polycrystals. Both these derivations assume that the distribution of orientations of the grains is continuous. This is the reason why the Enforced Uniform Distribution enter the Hashin-Shtrikman zone with a greater frequency than that of Uniform Probability Distribution. Since these bounds have been derived for an infinite assembly, if the Shear Modulus of an aggregate of polycrystals lies in this zone, it implies that the aggregate is showing the response that an infinite assembly would. This is observed in the Minimal boundary conditions. Thus, the Minimal boundary conditions simulate an infinite medium which provides an effective counter to the problems faced in computational mechanics due to End Effects.

6.2 Stress Distributions in the Crystalline Aggregate

The distributions for the in-plane Shear stress are presented in this section. These give a general idea of the areas of stress concentrations. The contours are plotted such that they compare with the overall elastic modulus i.e. they are plotted for each contour to lie within the bounds calculated for the crystalline aggregate.

In the contours shown below, the areas in black are where the stress value is below the Reuss (lower) bound. The dark and light blue areas denote the elements whose stress value lies between the Reuss bound and the Hashin-Shtrikman lower bound. The areas in green are where the stresses are within the Hashin-Shtrikman regime and the

yellow and the red areas denote the regions where the stress lies between the Upper Hashin-Shtrikman bound and the Voigt (Upper) bound.

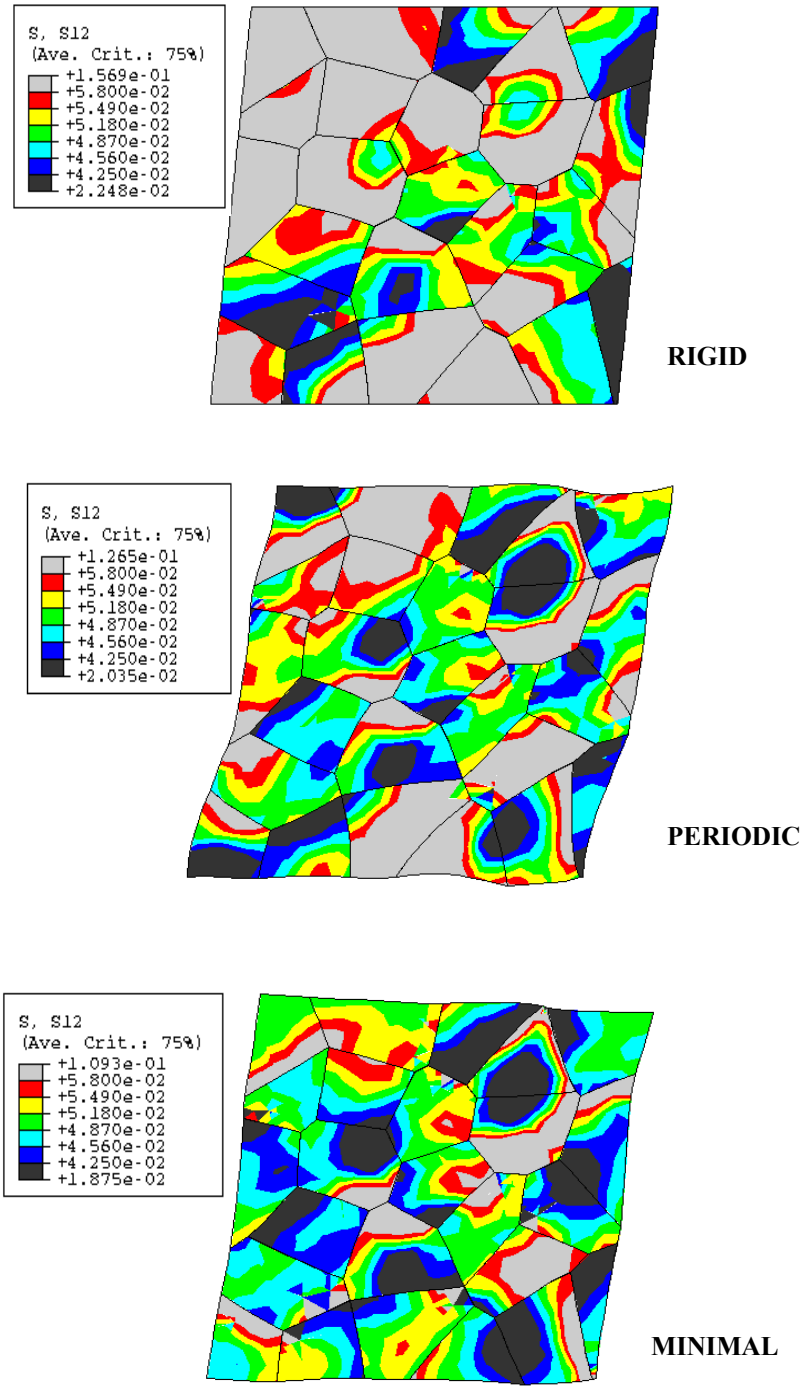

Fig 6.3 Stress Distributions in the 25 Crystal Aggregate

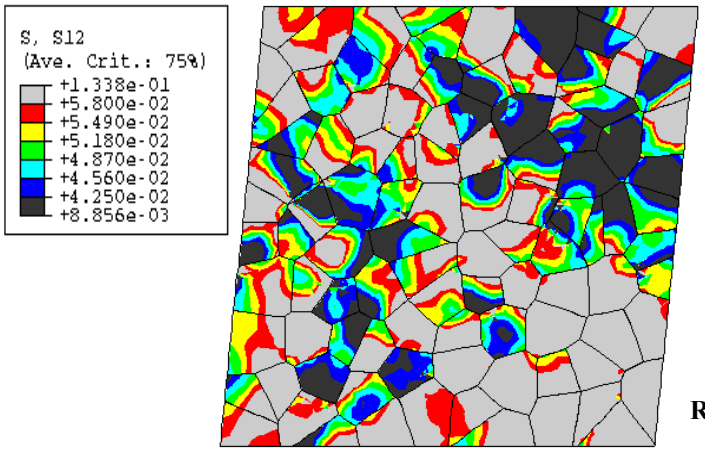

RIGID

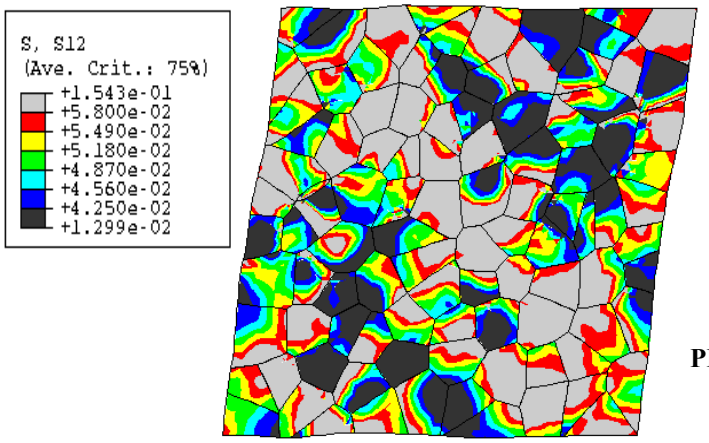

PERIODIC

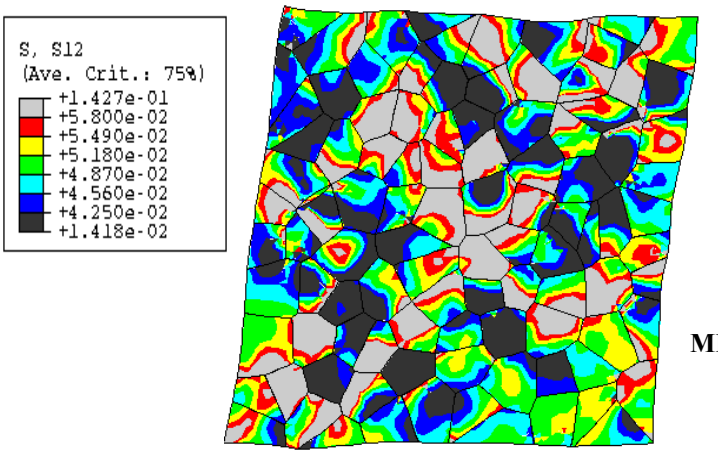

MINIMAL

Fig 6.3 Stress Distributions in the 100 Crystal Aggregate

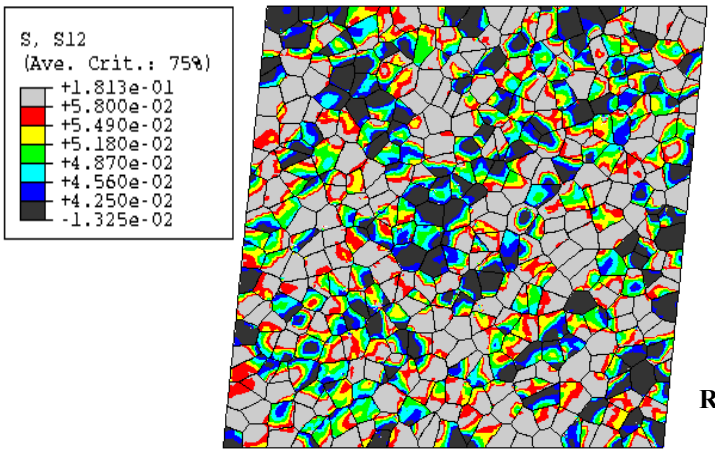

RIGID

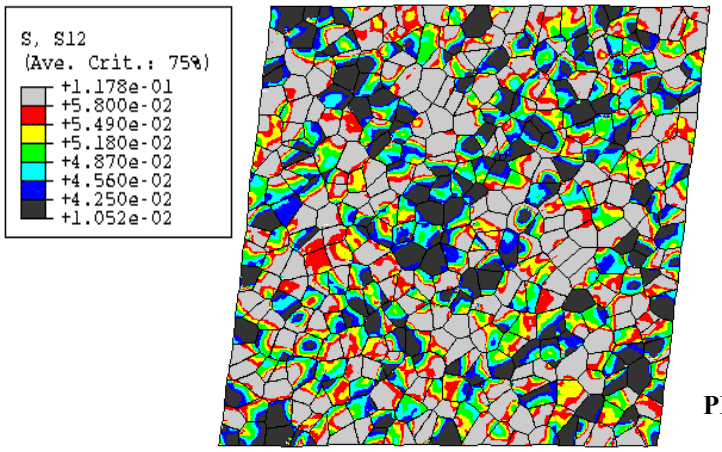

PERIODIC

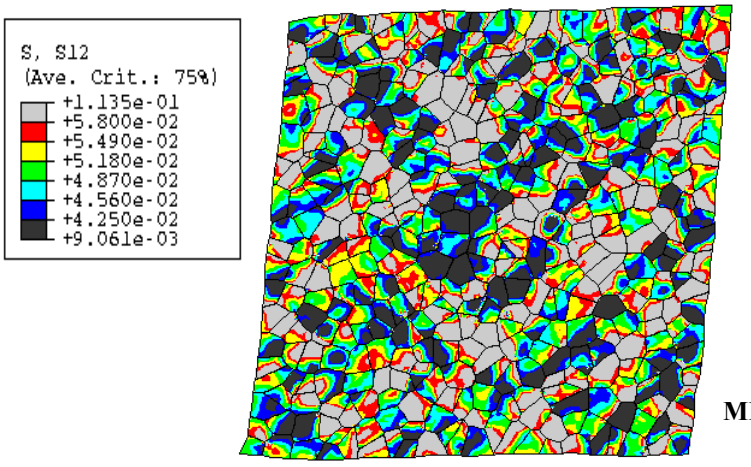

MINIMAL

Fig 6.3 Stress Distributions in the 400 Crystal Aggregate

The stress contours show that large portions of the assembly have stresses above the Voigt bound for the Rigid boundary conditions. Very few elements fall within the Hashin-Shtrikman regime which demonstrates the strictness of these boundary conditions. The Periodic boundary conditions are an improvement over the Rigid boundary conditions, but still contain substantial number of elements which have stress values outside the bounds (Voigt-Reuss). The Minimal boundary conditions provide stress contours in which majority of the assembly falls in the Voigt-Reuss Bounds.

The Minimal boundary conditions generate stresses which are largely confined to a relatively small segment of the stress spectrum. This phenomenon is observed for all the assemblies. As the size of the assembly increases, larger areas fall in this small domain of stresses. This is a definite trend towards homogeneity, a typical characteristic of macroscopic deformation. Thus, the Minimal boundary conditions overcome the constraint of a specimen of finite length.

6.3 Fourier Transforms

The Fourier Transform gives a mathematical perspective of the results. The Fourier Transform converts a given function from a time or space domain to a frequency or wavelength domain. Fourier Transform of the variations of stress from the average are performed in the current context. Since this is a function of space, the Fourier Transform converts it into a wavelength domain. It gives the dependence of the function for various wavelengths of the specimen. A two-dimensional Fourier Transform is performed here which accounts for periodicity of stress variations in both the x and y directions of the crystalline aggregate.

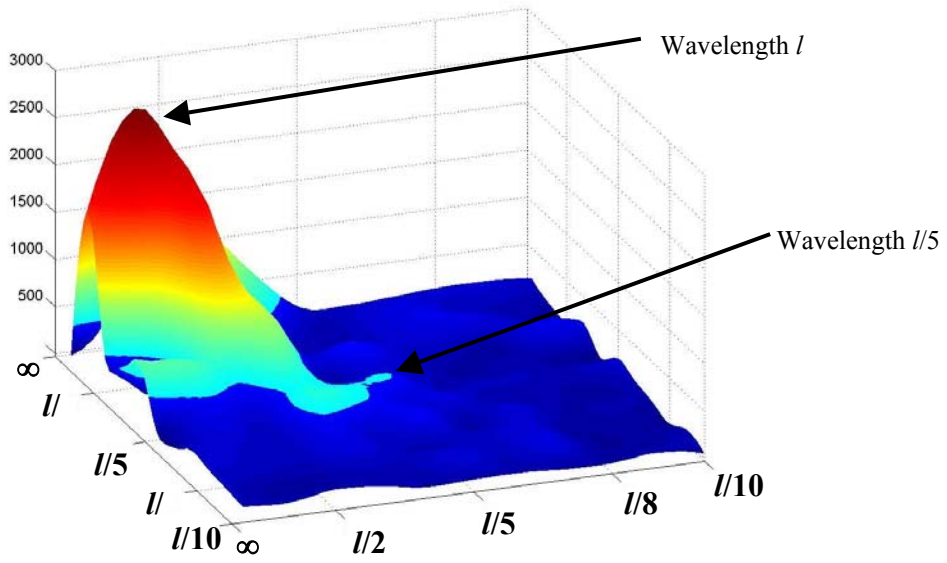

(a)

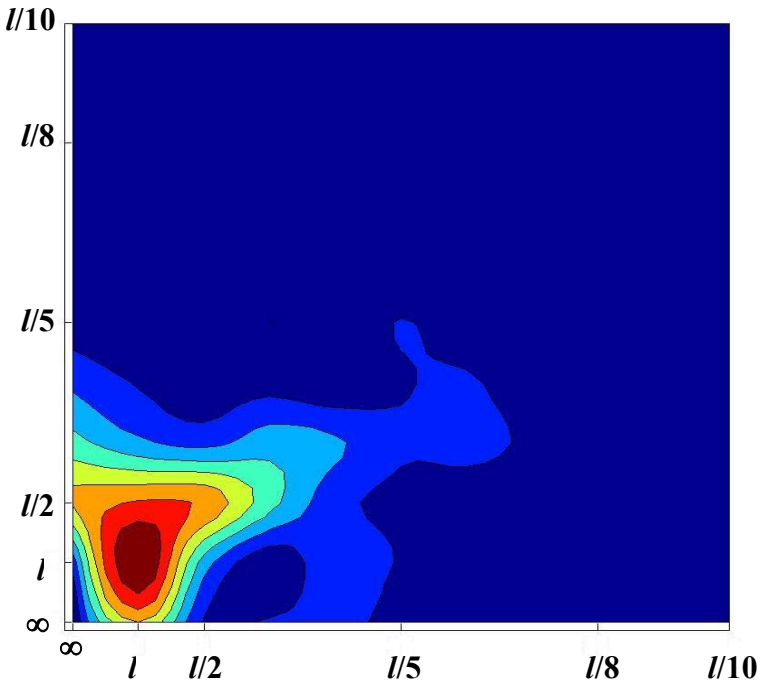

(b)

Fig. 6.6 Fourier Transforms for 25 grains assembly subjected to Rigid boundary conditions

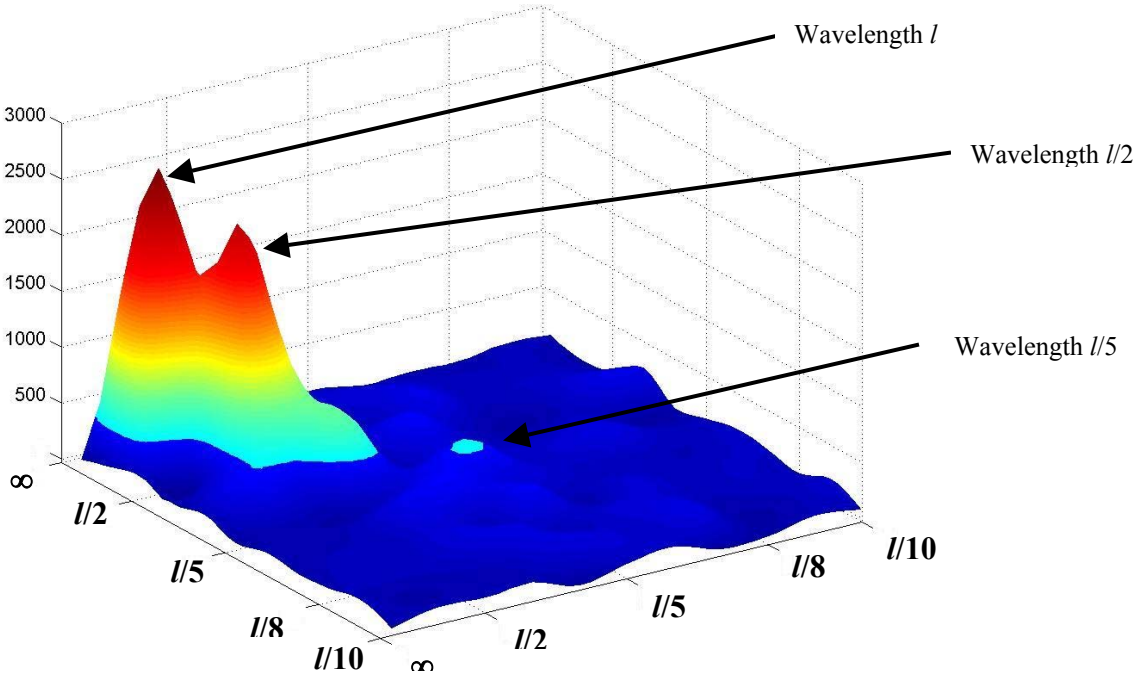

(a)

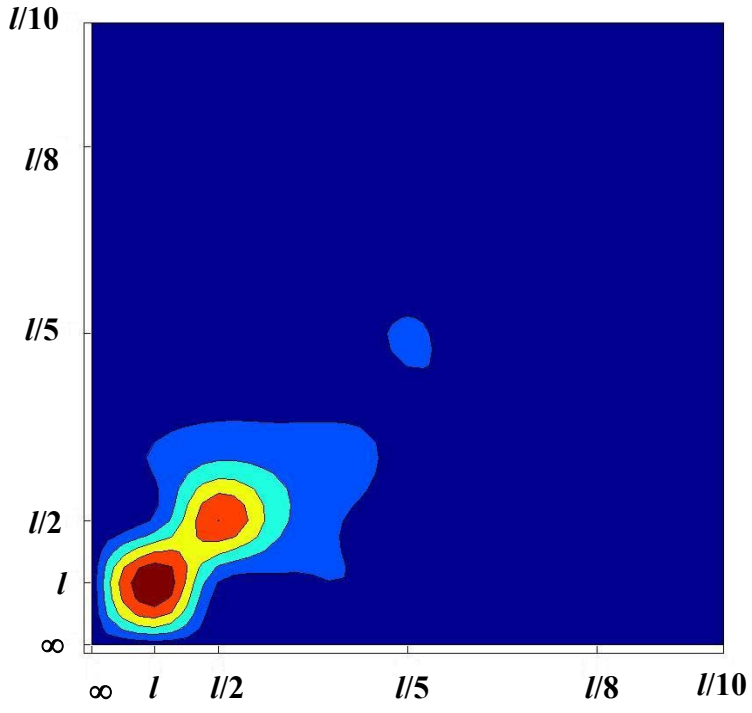

(b)

Fig. 6.7 Fourier Transforms for 25 grains assembly subjected to Periodic boundary conditions

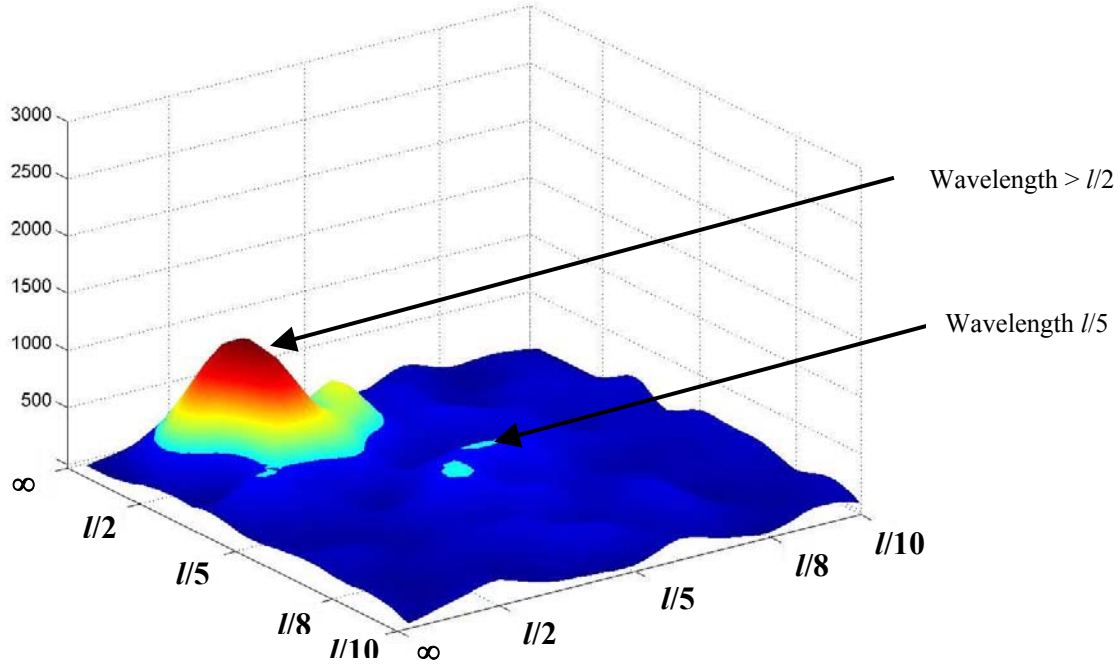

(a)

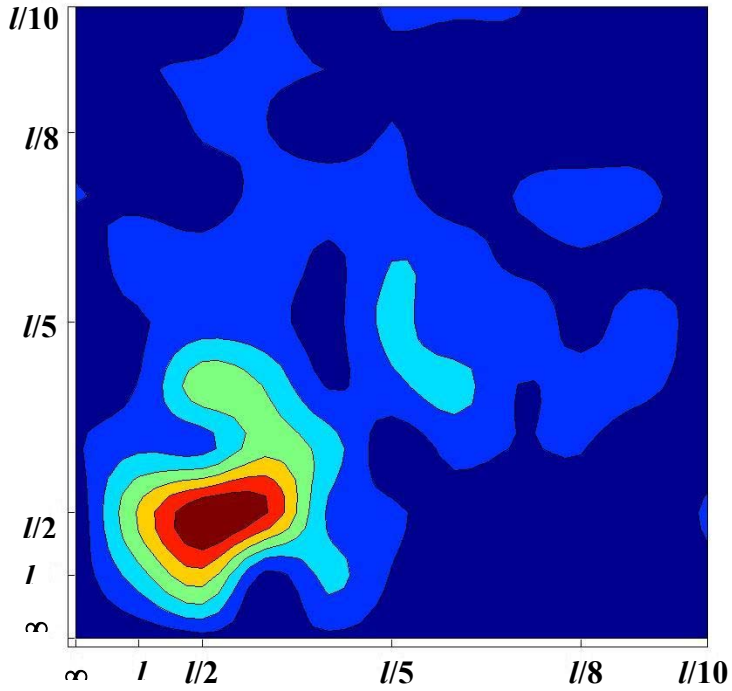

(b)

Fig. 6.8 Fourier Transforms for 25 grains assembly subjected to Minimal boundary conditions

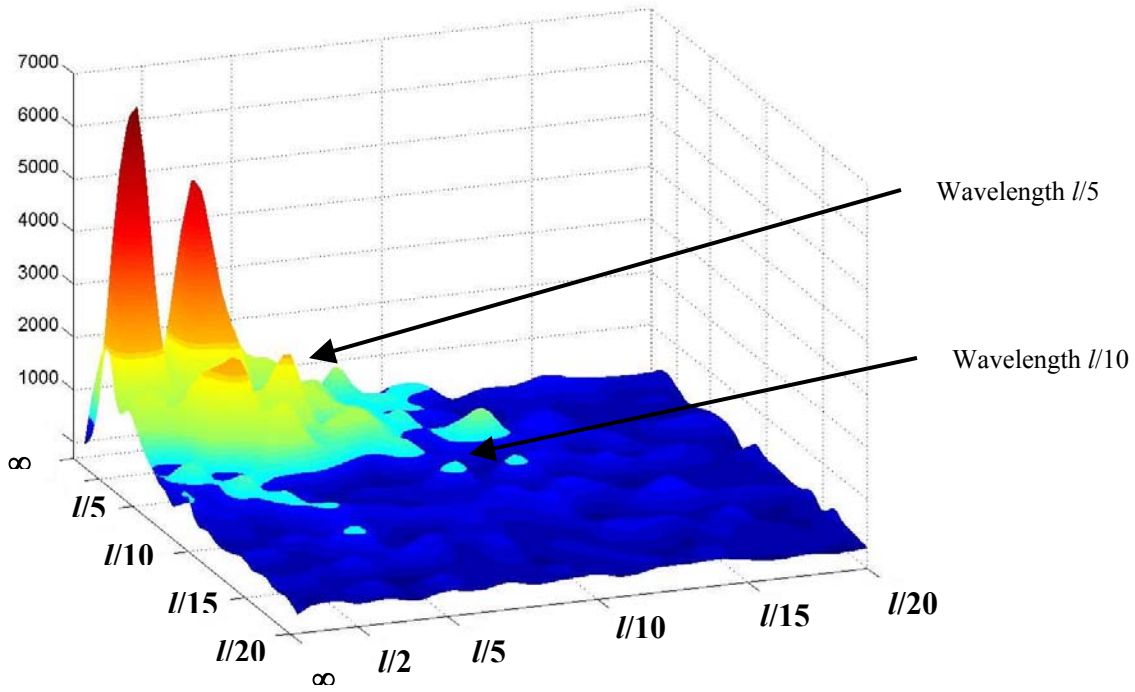

(a)

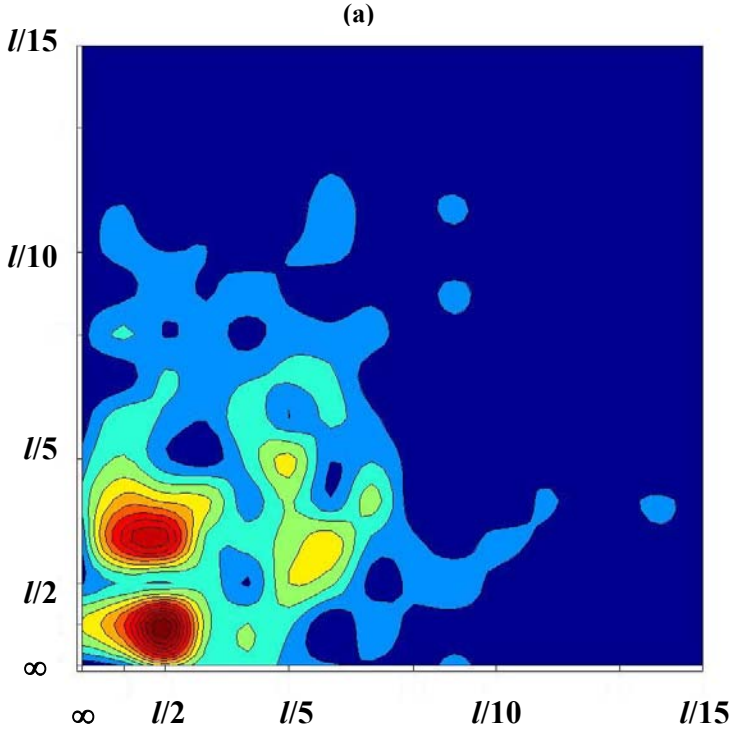

(b)

Fig. 6.9 Fourier Transforms for 100 grains assembly subjected to Rigid boundary conditions

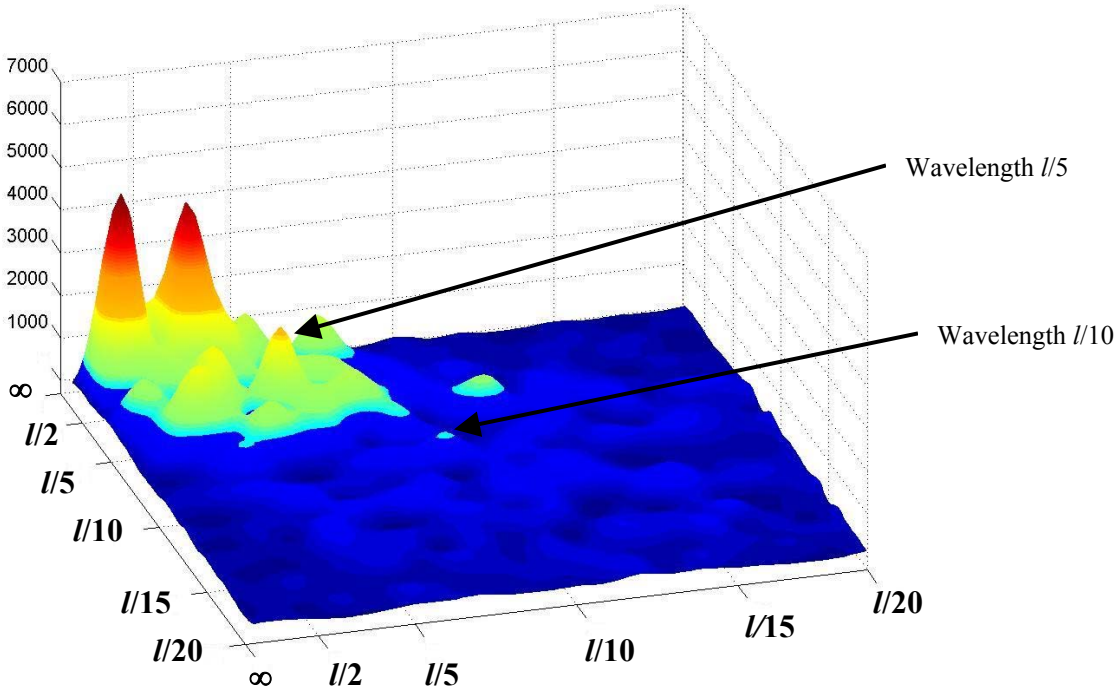

(a)

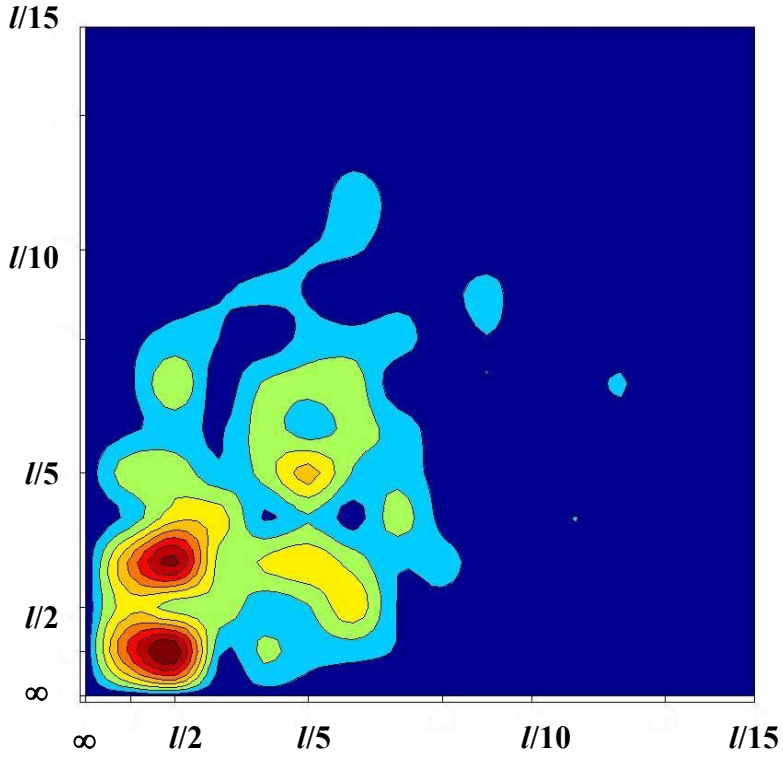

(b)

Fig. 6.10 Fourier Transforms for 100 grains assembly subjected to Periodic boundary conditions

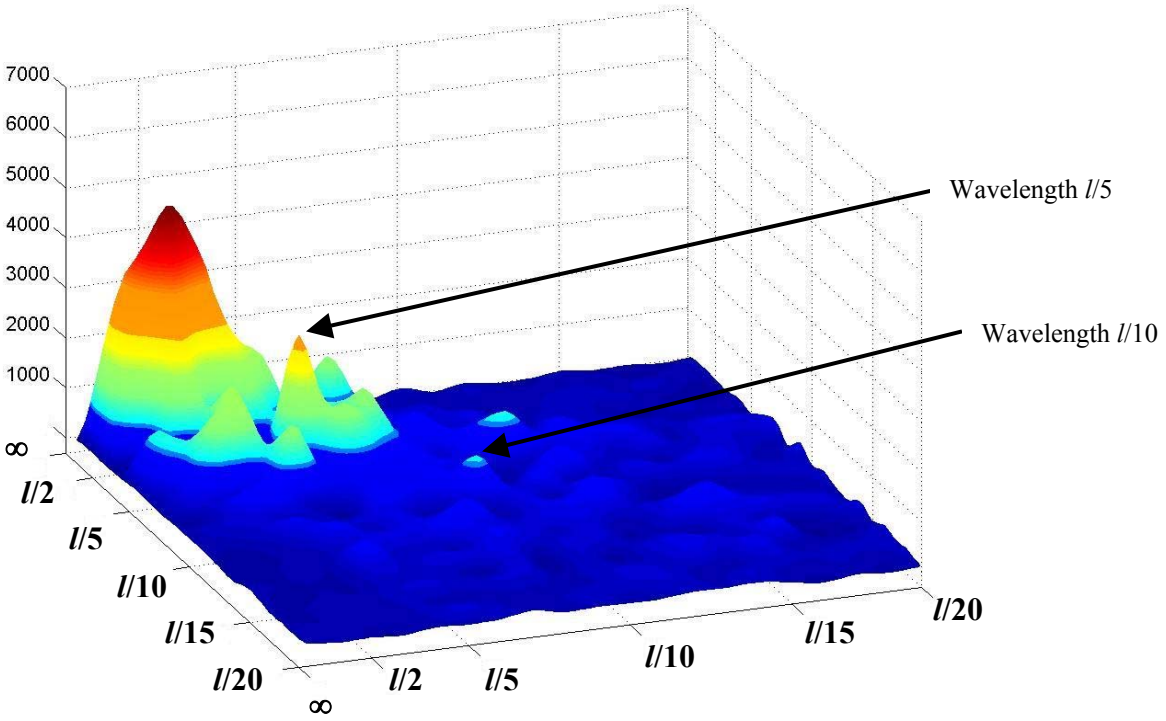

(a)

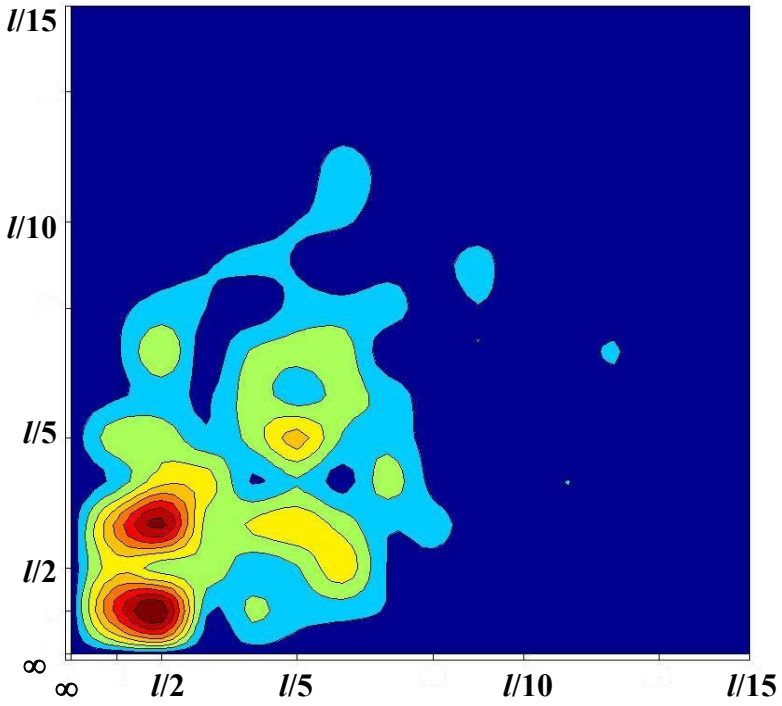

(b)

Fig. 6.11 Fourier Transforms for 100 grains assembly subjected to Minimal boundary conditions

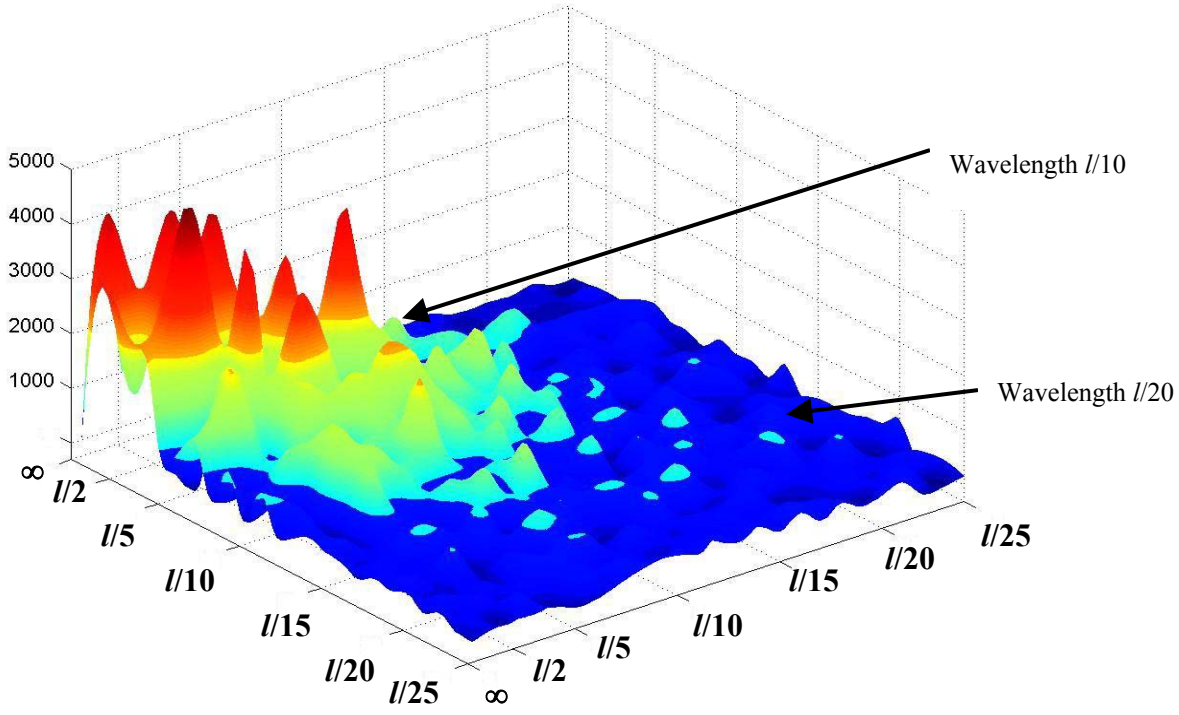

(a)

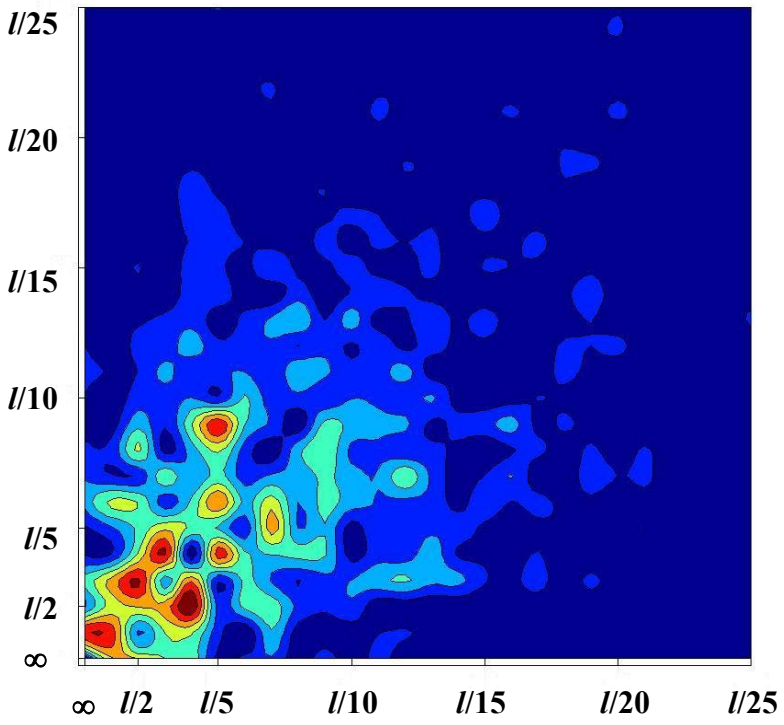

(b)

Fig. 6.12 Fourier Transforms for 400 grains assembly subjected to Rigid boundary conditions

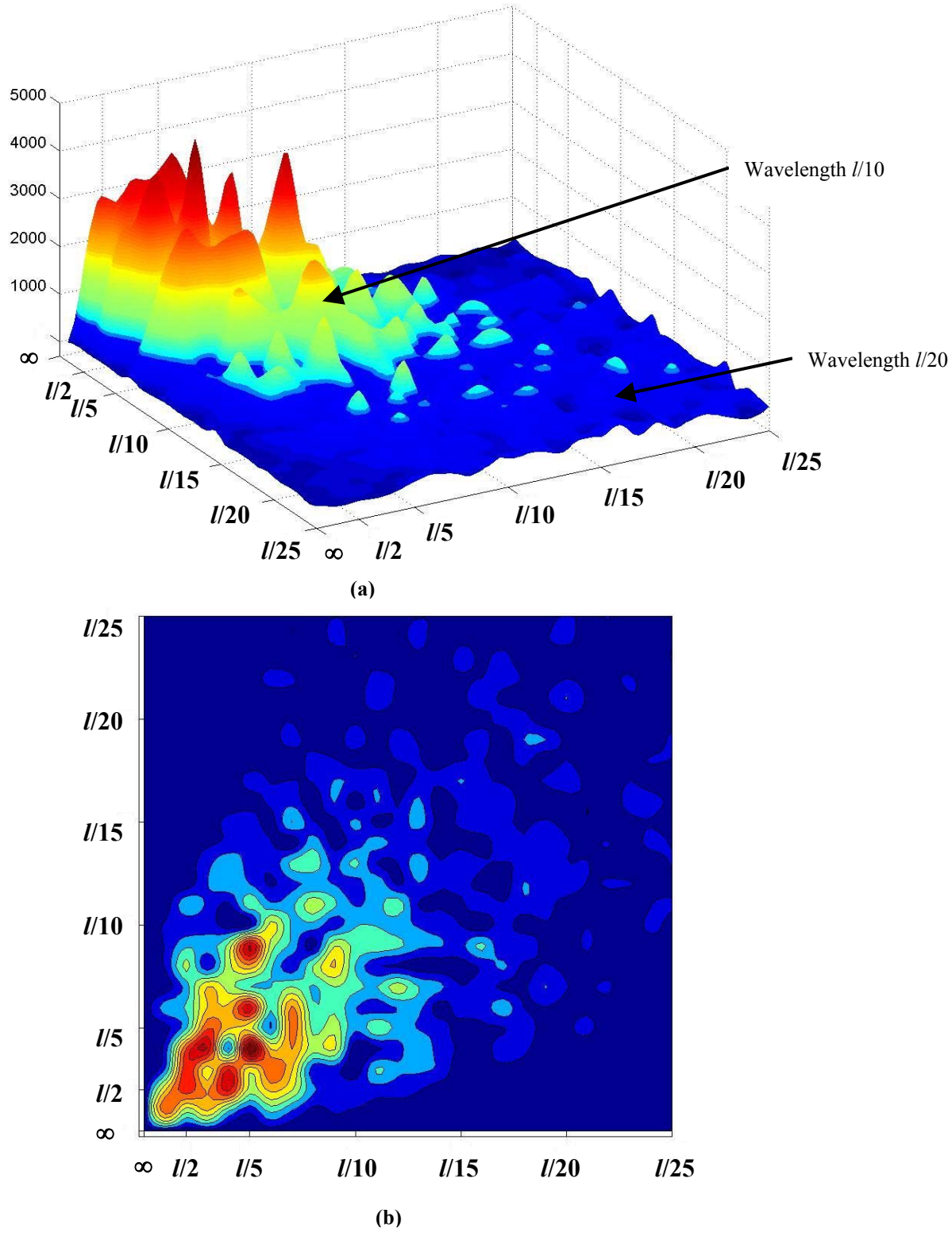

Fig. 6.13 Fourier Transforms for 400 grains assembly subjected to Periodic boundary conditions

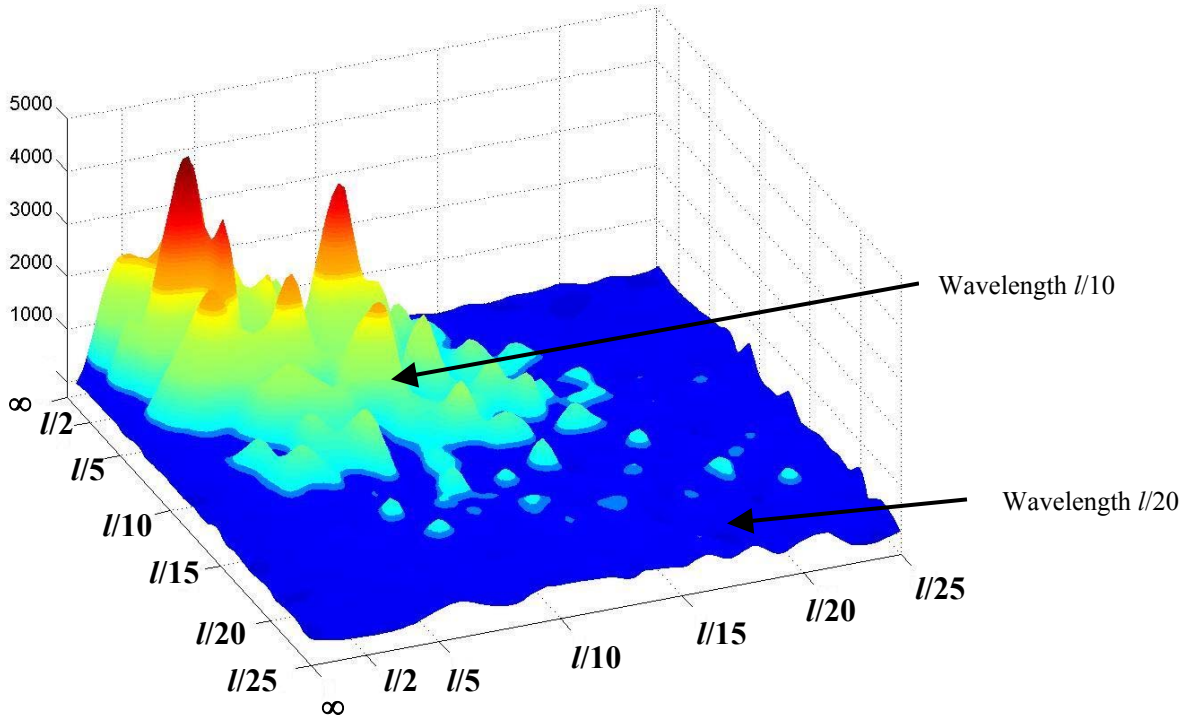

(a)

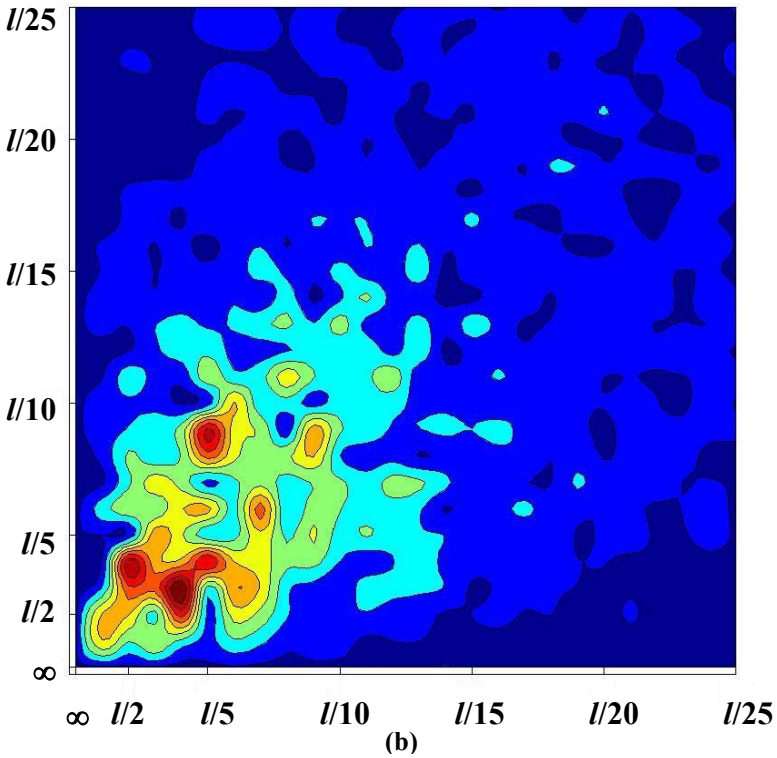

(b)

Fig. 6.14 Fourier Transforms for 400 grains assembly subjected to Minimal boundary conditions

The Fourier Transforms confirm to the expectations that the Minimal boundary conditions are more suitable for deformation simulation of materials.

For the 25 grains assembly, a very high peak is obtained at wavelength l and a peak is noticed at the wavelength $l/5$ for the Rigid boundary conditions. This indicates that the field variables (stress) are highly dependent on the size of the specimen, which should not happen. The Periodic boundary conditions also give a strong peak at wavelength l, but slightly smaller in magnitude. This is because both boundary conditions impose periodicity of the RVE. The periodic boundary conditions also generate peaks at a wavelength slightly lesser than $l/2$ and at the wavelength $l/5$. The Minimal boundary conditions do not exhibit a sizeable peak at wavelength l, but yield peaks at wavelengths slightly lesser than $l/2$ and at wavelength l. The peak displayed at a wavelength $l/5$ is for a wavelength corresponding to one grain. Since the Fourier Transform of the variations of stress is performed, there will be a peak at a wavelength corresponding to an integral multiple of one grain since the stress varies from one grain to another. Further, the Periodic and Minimal boundary conditions exhibit peaks at wavelengths slightly lesser than $l/2$ i.e. slightly lesser than 2.5 grains. Thus, peaks are exhibited at wavelengths very close to twice the grain size.

For the 100 grains assembly, the trends continue i.e. the magnitude of the peak at a wavelength l is lesser for the Minimal boundary conditions than for the Rigid and Periodic boundary conditions. Peaks are observed at wavelengths $l/10$, $l/5$ and $l/2$ for all the cases. These correspond to wavelengths of one grain size, two grain sizes and five grain sizes respectively. Also, off-diagonal peaks are observed at wavelengths $l/5$ and $l/2$.

This implies that the variation of the field variable (stress) is periodic in one particular direction i.e. in one particular direction, the orientations assigned to the grains have attained periodicity which causes the periodic variations of stress and thus produces high peaks at these wavelengths.

For the 400 grains assembly too, the peaks at wavelength *l* are much lower for Minimal boundary conditions than for Rigid and Periodic boundary conditions at the same wavelength. As in the case of the 100 grains assembly, off-diagonal peaks are observed for all the boundary conditions at wavelength *l*/2 (in one direction) and wavelength *l*/5 (in both the directions). This implies a periodicity of orientations at the corresponding wavelengths.

The most important fact to be realized is the lower peaks of the Minimal boundary conditions for wavelength l. This implies that the stresses are not dependent on the size of the computational model. The Size Effect inherent to both the other boundary conditions has been reduced by a large extent.

CHAPTER 7

CONCLUSIONS

The computational models are subjected to the different boundary conditions and the results are analyzed. The Rigid boundary conditions demonstrate the stiffest response followed by the Periodic boundary conditions and the Minimal boundary conditions. This is attributed to the additional rigidity and/or periodicity of the boundary conditions in the first two cases.

The distribution of the results for overall shear modulus is over a wider range for uniform probability distribution of orientations. The range of the results narrows as the number of grains increase. This shows the tendency of the computational model to demonstrate a behavior of an infinite media. In the case for an infinite media, the three boundary conditions would yield the same response.

The shear modulus values of a 100 grain assembly subjected to Minimal boundary conditions enters the Hashin-Shtrikman regime, whereas the response of even the 400 grain assembly lies outside the Hashin-Shtrikman zone for Rigid and Periodic boundary conditions. Thus the Minimal boundary conditions require a much smaller computational cell size and effectively overcome end effects.

The Fourier Transforms of the stress variations indicate that the Minimal boundary conditions do not introduce spurious wavelengths like Rigid or Periodic boundary conditions. Strain gradients and/or localization can also be simulated using these boundary conditions.

REFERENCES

1. Bishop J. F. W, Hill R, *A Theory of the Plastic Distortion of a Polycrystalline Aggregate under Combined Stresses*, Phil. Mag., 1951
2. Gurson A.L, *Continuum Theory of Ductile Rupture by Void Nucleation and Growth: Part 1-Yield Criteria and Flow Rules for Porous Ductile Media*, Transactions of the ASME, 1977
3. Hashin Z, Shtrikman S*, On Some Variational Principles in Anisotropic and Nonhomogeneous Elasticity*, Journal of the Mechanics and Physics of Solids, 1962
4. Hashin Z, Shtrikman S, *A Variational Approach to the Theory of the Elastic Behaviour of Polycrystals*, Journal of the Mechanics and Physics of Solids, 1962
5. Kanit T, et al, *Determination of the Size of the Representative Volume Element for Random Composites: Statistical and Numerical Approach, International Journal of Solids and Structures*, 2003
6. Hughes T.J.R, *The Finite Element Method*, Dover Publications, 2000
7. Malvern L. E, *Introduction to the Mechanics of a Continuous Medium*, Prentice-Hall, 1969
8. Brigham O. E, *The Fast Fourier Transform and its Applications*, Prentice-Hall, 1988
9. Nye J. F, *Physical Properties of Crystals*, Oxford Science Publications, 1995